## Beamline 4.0.2

# Magnetic Spectroscopy

### A study of acetyl-CoA decarbonylase/Synthase using x-ray magnetic circular dichroism at beam line 4.02 of the ALS

Funk, T., S. Friedrich, W. Gu, D.A. Grahame, S.P. Cramer

### Circular dichroism in K-shell ionization from fixed-in-space CO and $N_2$ molecules

Jahnke, T., Th. Weber, A.L. Landers, A. Knapp, S. Schössler, J. Nickles, S. Kammer, O. Jagutzki, L. Schmidt, A. Czasch, T. Osipov, E. Arenholz, A.T. Young, R. Díez Muiño, D. Rolles, F.J. García de Abajo, C.S. Fadley, M.A. Van Hove, S.K. Semenov, N.A. Cherepkov, J. Rösch, M.H. Prior, H. Schmidt-Böcking, C.L. Cocke, R. Dörner

### Comparison of magnetic anisotropy by x-ray magnetic linear dichroism

Ohldag, H., S. Maat, E. Arenholz, A.T. Young, A. Scholl, B.A. Gurney, J. Stöhr

### Correction of non-linearity in detectors for electron spectroscopy

Mannella, N., S. Marchesini, S.-H. Yang, B.S. Mun, A.W. Kay, T. Gresch, A. Rosenhahn, C.S. Fadley

### Development of a GHz-rate detector for synchrotron radiation research

Turko, B., M. Press, A.W. Kay, M. West, J.E. Katz, H. Spieler, Z. Hussain, C.S. Fadley, B. Ludewigt, J.-M. Bussat, P. Denes, H. von der Lippe, G. Meddler, G. Zizka, G. Lebedev, M. Mellon, T. Wiell

### Magnetic circular dichroism in the x-ray absorption spectra of the CMR compound, $Yb_{14}MnSb_{11}$

Holm, A.P., S.M. Kauzlarich, S.A. Morton, G.D. Waddill, W.E. Pickett, J.G. Tobin

### Magnetic properties of $Fe_3O_4$ films grown by epitaxial electrodeposition on the low index planes of gold

Switzer, J.A., T.A. Sorenson, S.A. Morton, G.D. Waddill

### Magnetic properties of uncompensated spins in Co/NiO

Ohldag, H., F. Nolting, E. Arenholz, A. Scholl, A.T. Young, S. Maat, M. Carey, J. Stöhr

### Mechanisms of photo double ionization of helium by 530 eV photons

Knapp, A., A. Kheifets, I. Bray, Th. Weber, A.L. Landers, S. Schössler, T. Jahnke, J. Nickles, S. Kammer, O. Jagutzki, L.Ph. Schmidt, T. Osipov, J. Rösch, M.H. Prior, H. Schmidt-Böcking, C.L. Cocke, R. Dörner

### Multi-atom resonant photoemission effects from solid surfaces and free molecules

Mannella, N., B.S. Mun, S.-H. Yang, A.W. Kay, F.J. Garcia de Abajo, E. Arenholz, A.T. Young, Z. Hussain, H. Wang, O. Hemmers, D.W. Lindle, M.A. Van Hove, C.S. Fadley

### Resolving magnetic and chemical correlation lengths in CoPtCr-based recording media

Hellwig, O., D.T. Margulies, B. Lengsfield, E. E. Fullerton, J.B. Kortright

### Spin-resolved electron spectroscopy of carbonyl sulphide

Turri, G., G. Snell, B. Langer, M. Martins, E. Kukk, P. Langhoff, N. Berrah

### Variable moments and changing magnetic behavior of thin-film FeNi alloys

Hochstrasser, M., J.G. Tobin, N.A.R. Gilman, R.F. Willis, S.A. Morton, G.D. Waddill

# A Study of Acetyl-CoA Decarbonylase/Synthase Using X-Ray Magnetic Circular Dichroism at Beam Line 4.02 of the ALS

**T. Funk[1], S. Friedrich[1], W. Gu[2], D.A. Grahame[3] and S. P. Cramer[1,2]**

[1]Lawrence Berkeley National Lab, Cyclotron Road 1, Berkeley, CA 94720 USA
[2]Department of Applied Science, UC Davis, One Shields Avenue, Davis, CA 95616 USA
[3]Dept. of Biochemistry and Molecular Biology, USUHS, 4301 Jones Bridge Road, Bethesda, MD 20814 USA

## INTRODUCTION

X-ray magnetic circular dichroism (XMCD) spectroscopy provides a unique opportunity to study spin and oxidation states of dilute transition metals in metallo proteins. Advantages of the technique include element selectivity and high sensitivity.
The XMCD signal is given by the difference in absorption between right and left circular polarized X-rays [1]. XMCD probes the population of the magnetically split levels by measuring the difference in absorption between right and left circular polarized X-rays. Since in paramagnetic systems this population is given by Boltzmann statistics, XMCD requires high fields and low temperatures.
Applying the sum rules to the measured spectra allows determining the spin and the orbital angular momentum of the metal centers [2]. Furthermore, one can observe the signal as function of the magnetic field to get magnetization curves of the system. This allows to extract the total angular momentum and the g-factor of the specific metal sites by fitting a Brillouin function. This also provides information, if various chemical species of the same element are present.
We have studied the active site of the enzyme acetyl-CoA decarbonylase/synthase (ACDS) using this method. ACDS contains 5 protein subunits and catalyzes the cleavage (or synthesis) of acetyl-CoA [5]. In the current model, the active site A cluster (which is located on the ACDS β subunit) contains an Fe-S cluster with a Ni atom bridged to it [3]. During the catalytic cycle of ACDS the Ni and the Fe sites change the oxidation state. An important step to understand the catalyzes is to understand the various steps in the catalytic cycle.

## EXPERIMENTS

With our current setup located at the elliptically polarized undulator beam line of the ALS we can study systems with a metal concentration of 500 ppm and below utilizing a commercial 30 element Ge detector. Our endstation hosts a 6 Tesla superconducting magnet cooled with liquid helium. The sample is located in the bore of the magnet and is attached to a separate pumped $^{4}$He cryostat providing sample temperatures of 2.2 K [4].
The proteins are prepared in a dried film on a sapphire disk in a glove box. The sample is transferred to the experimental chamber and cooled to base temperature in a specially designed capped sample holder.
We prepared ACDS β sununit in 2 states important for the catalyzes. One state was obtained by reducing the protein with Ti citrate and another was obtained treating the reduced protein with CO.
The magnetic response was studied at the Ni and the Fe sites recording the respective L-edges with circularly polarized light at 2.2K and 6T.

## RESULTS AND DISCUSSION

Ti citrate reduced ACDSβ shows a strong magnetic signal in the Ni as well as in the Fe spectrum.

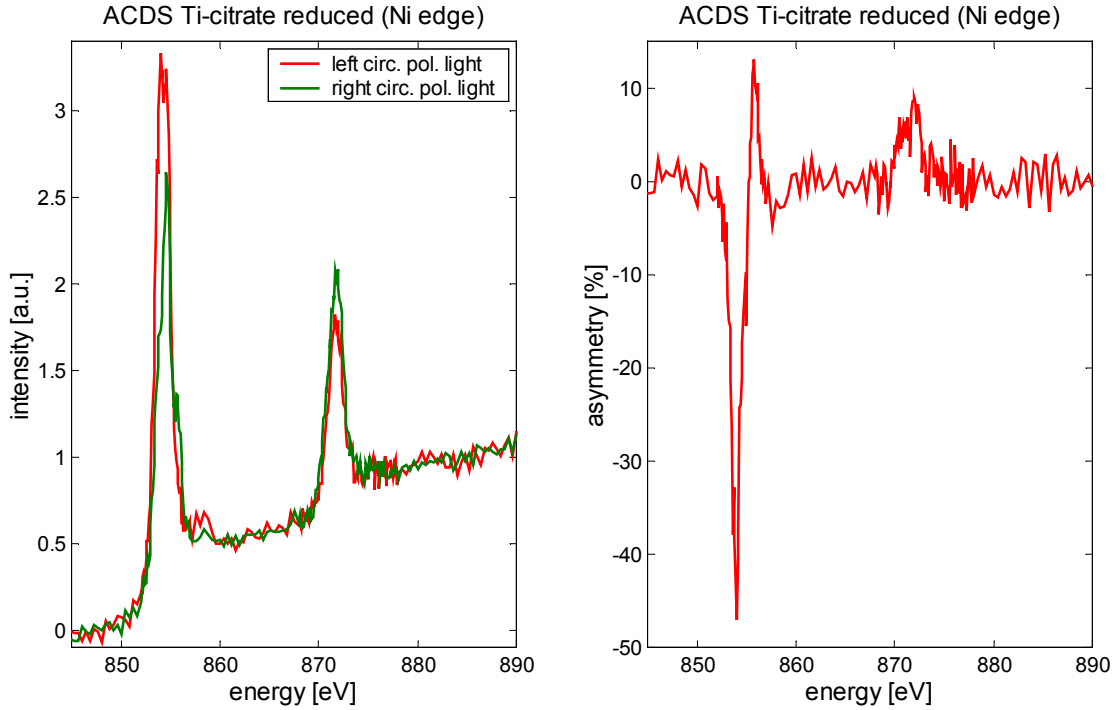


Figure 1a and 1b: L-edge spectra with right and left circularly polarized light (a). Difference of with right and left circularly polarized light spectra and normalized to maximum of L-edge spectrum (b).

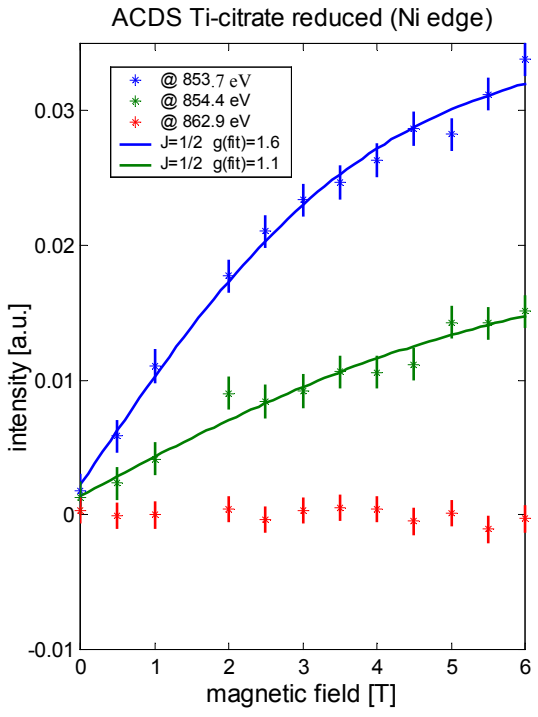


Figure 2: Magnetization curves at different excitation energies. The red curve was taken between the L3 and L2 line and shows no signal

Figure 1a shows the L-edge spectra of Ni for left and right circularly polarized light. Figure 1b shows the XMCD signal taking the difference spectrum between left and right circularly polarized light normalized with the maximum of the L-edge spectra leading to an XMCD effect of around 50%. Magnetization curves were taken at various excitation energies as shown in figure 2. One curve was measured at 862.9 eV just between the L3 and L2 lines. Since no magnetic response is expected at this position this curve determines the base line. Another set of curves were taken at two positions of the L3 line. Fits of the Brillouin function to the data results in different g-values. This indicates the presence of different chemical species of Ni in the sample with different magnetic properties. The measured spectrum is a superposition of the spectra of the different species. A similar behavior was observed for the magnetization curves taken at the Fe edge. The L3 edge is

showing a double peak feature with both peaks exhibiting a strong magnetic response. The maximum XMCD signal is about 35%.
Treating the sample with CO changes the resulting spectra dramatically. The magnetic signal on the Ni site disappears almost completely. A residual XMCD signal of 10% is observed. Also the XMCD signal of the Fe is drastically reduced to about 20%. The double peak feature at the L3 line also disappears. A magnetization curve was taken at the excitation energy of the maximum Fe-XMCD signal revealing a magnetization close to saturation. This rules out that the XMCD signal disappeared due to insufficient thermal contact.

## ACKNOWLEDGEMENTS

The NIH through Grant No. GM4430 and the Department of Energy, Office of Biological and Environmental Research supported this work. For excellent support we like to thank Tony Young, Elke Arenholz, and Rene Delano and the staff of the ALS.

## REFERENCES

[1] J. Stöhr and Y. Wu in: New Directions in Research with Third-Generation Soft X-Ray Synchrotron Radiation Sources, Eds. A.S. Schlachter and F. J. Wuilleumier, Kluwer Academic Publishers (1994), 221
[2] S. Cramer *et al.,* ACS symposium series 692, **154** (1997)
[3] S. W. Ragsdale, and M. Kumar, *Chem. Rev.* **96**, 2515 (1996)
[4] T. Funk, S. Friedrich, A. Young, E. Arenholz and S. P. Cramer, RSI **73,3** (2002)
[5] B. Bhaskar, E. DeMoll, and D.A. Grahame, *Biochemistry* **37,** 14491-14499 (1998)

Principal investigator: Stephen P. Cramer, Department of Applied Science, UC Davis, and Ernest Orlando Lawrence Berkeley National Laboratory. E-mail: cramer@lbl.gov, telephone: 510-486-4720.

# Circular Dichroism in K-shell Ionization from Fixed-in-Space CO and $N_2$ Molecules

T. Jahnke[1], Th. Weber[1], A.L. Landers[2], A. Knapp[1], S. Schössler[1], J. Nickles[1], S. Kammer[1], O. Jagutzki[1], L. Schmidt[1], A. Czasch[1], T. Osipov[3], E. Arenholz[4], A.T. Young[4], R. Díez Muiño[5,6], D. Rolles[5], F.J. García de Abajo[5], C.S. Fadley[5,7], M.A. Van Hove[4,5,7], S.K. Semenov[8], N.A. Cherepkov[8], J. Rösch[9], M.H. Prior[9], H. Schmidt-Böcking,[1] C.L. Cocke,[3] and R. Dörner[1]

[1] Institut für Kernphysik, University Frankfurt, August-Euler Str 6, D-60486 Frankfurt Germany
[2] Dept. of Physics, Western Michigan Univ., Kalamazoo, MI 49008, USA
[3] Dept. of Physics, Kansas State Univ, Cardwell Hall, Manhattan, KS 66506, USA
[4] Advanced Light Source, Ernest Orlando Lawrence Berkeley National Laboratory, University of California, Berkeley, California 94720, USA
[5] Materials Sciences Division, Ernest Orlando Lawrence Berkeley National Laboratory, University of California, Berkeley, California 94720, USA
[6] Donóstia International Physics Center, P. Manuel de Lardizabal 4, 20018 San Sebastián, Spain
[7] Department of Physics, University of California, Davis, CA 95618, USA
[8] State University of Aerospace Instrumentation, 190000 St. Petersburg, Russia
[9] Chemical Sciences Division, Ernest Orlando Lawrence Berkeley National Laboratory, University of California, Berkeley, California 94720, USA

## INTRODUCTION

This project studies photoemission (photoionization) from "fixed-in-space" molecules, comparing measured angular distributions with theory. In particular, strong circular dichroism in angular distribution (CDAD) is measured for CO and $N_2$, which is explained by calculations performed both in the multiple-scattering and random-phase-approximation formalisms. The new CDAD measurements, together with earlier results with linearly polarized photons [1,2], constitute the most complete description of K-shell photoemission from a free diatomic molecule. They provide benchmark tests of theoretical methods that are indispensable, for example, in the interpretation of photoemission and photoelectron diffraction data from solids.

## METHODS

The present experiment was performed using COLTRIMS (Cold Target Recoil Ion Momentum Spectroscopy [3]) at elliptically polarized undulator beamline 4.0.2 of the Advanced Light Source. The resolution for the photoelectron ranges from 1-3 eV depending upon its energy; this is sufficient to discriminate the direct K-shell photoelectron from the Auger and satellite shake up electrons. In the analysis we have used for CO only the $C^+ + O^+$ decay channel with a kinetic energy release KER > 10.2 eV [2], and for $N_2$ all ions from the $N^+ + N^+$ decay channel.

The calculations for CO are performed in a one-electron model using multiple scattering theory in non-spherical self-consistent potentials (MSNSP) [4] using the experimental values of the electron energy. The molecular ionic potential is split into two touching roughly hemispherical cells in which the full self-consistent potential is present. This allows us to include regions of space neglected by standard multiple scattering theory, and to avoid the usual spherical symmetrization of the potentials around each atomic scattering center. The inclusion of non-spherical effects has been found to be crucial in the calculation of the photoelectron angular distributions for kinetic energies of the electron lower than approximately 30 eV [3].

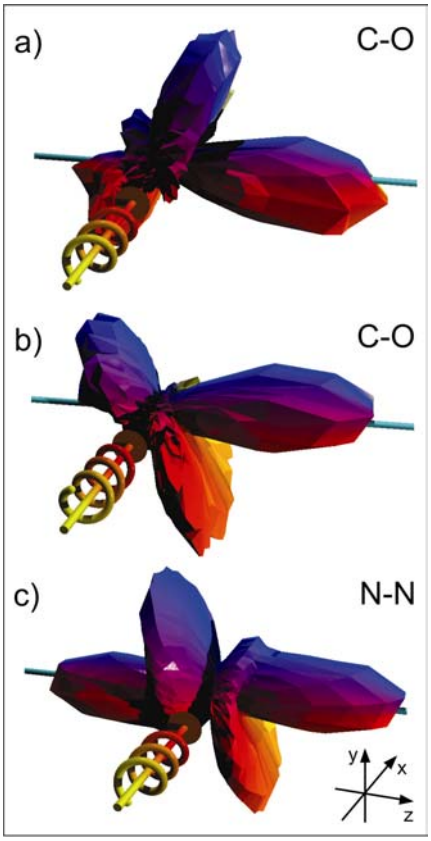


Figure 1. (a) and (b) -- Angular distributions of C(1s) photo-electrons (10 eV kinetic energy, on shape resonance) emitted from a CO molecule by absorption of left and right circularly polarized photons. The sense of rotation of the polarization vector is indicated by the spiral, where the photon propagation vector lies along the + x-axis (i.e., into the page) in all cases. The molecule is aligned along the z-axis, with the carbon atom at negative z in panels (a) and (b). Each vertex of the three-dimensional shape represents one data point. The data have not been smoothed, with the maximum corresponding to about 1000 counts. (c) -- Analogous distribution of N(1s) photoelectrons (9 eV, on resonance) from $N_2$.

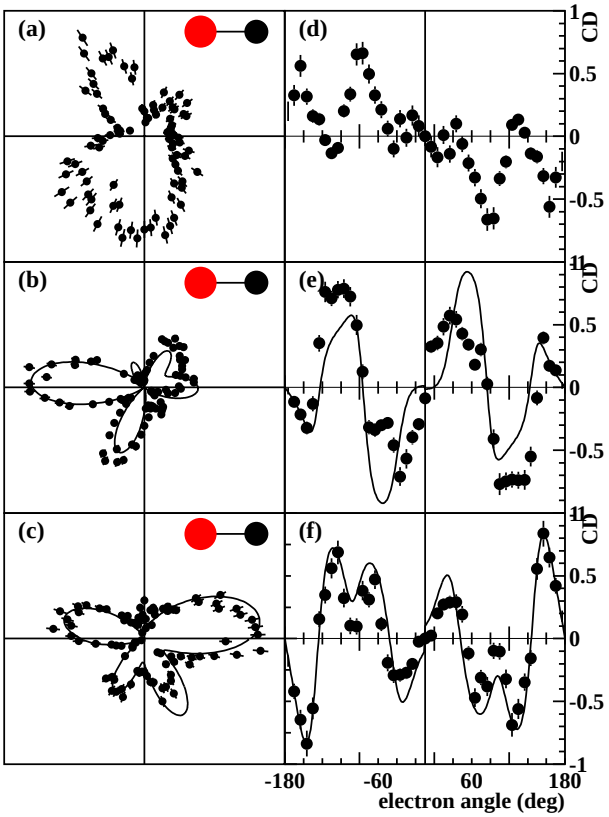


Figure 2. (a-c) Angular distribution of C(1s) photo electrons emitted from a CO molecule by absorption of right circularly polarized photons where the propagation vector of the light is into the page. The molecule lies along the horizontal axis as indicated, and both electrons and molecules lie within 10 degrees of the plane of the page. The electron energies are (a) 1.6, (b) 10.0 and (c) 24.6 eV. Panels (d-f) show the corresponding circular dichroism as defined in the text. Electron angle 0 corresponds to the direction of the carbon. Full lines: Theoretical multiple scattering calculations for the two higher energies, convoluted with the experimental resolution.

For $N_2$, the calculations take many-electron correlations into account in the Random Phase Approximation (RPA) [5,6]. In this approach, the non-spherical relaxed core Hartree-Fock potential is used as the zero order approximation for the photoelectron wave functions, and the coupling between the 1σ-g and 1σ-u channels is included within the RPA method.

## RESULTS

More quantitatively, Fig. 2 shows the photoelectron angular distribution from CO in the y-z-plane (perpendicular to the photon propagation) where CDAD is strongest. The molecule lies along the horizontal axis, as shown in the schematic, and the photon propagation vector is into the page. The electron energies are 1.6, 10.0 and 24.6 eV. The carbon-K σ shape resonance

results in a maximum of the cross section at around 10 eV (306 eV photon energy). The right panels show the CDAD defined as:

$$CDAD = (\sigma_{RCP} - \sigma_{LCP}) / (\sigma_{RCP} + \sigma_{LCP})$$

The theoretical calculations corresponding to the measurements are shown in Fig. 2 by the solid lines, using the multiple-scattering formalism: good overall agreement between experiment and theory is found.

Similar agreement between experiment and theory was obtained (not shown) for $N_2$, in which case the random-phase-approximation approach was used.

## ACKNOWLEDGMENTS

This work was supported in part by BMBF and DFG. R.D. was supported by the Heisenberg Programm der DFG, the Alexander von Humboldt and the Adolf Messer Stiftung. Th.W. thanks Graduiertenförderung des Landes Hessen for financial support. We thank Roentdek GmbH (www.Roentdek.com) for support with the delayline detectors. S.K.S. and N.A.C. acknowledge the financial support of the INTAS-RFBR grant (IR-97-471). R.D. acknowledges many enlightening discussions with J. Berakdar on the relationship of CDAD to phase information.

## REFERENCES

1. A. Landers, T. Weber, I. Ali, A. Cassimi, M. Hattass, O. Jagutzki, A. Nauert, T. Osipov, A. Staudte, M.H. Prior, H. Schmidt-Böcking, C.L. Cocke, and R. Dörner, Phys. Rev. Lett. **87**, 013002.
2. T. Weber, O. Jagutzki, M. Hattass, A. Staudte, A. Nauert, L. Schmidt, M. Prior, A. Landers, A. Bräuning-Demian, H. Bräuning, et al, J. Phys. **B34**, 3669 (2001).
3. R. Dörner, V. Mergel, O. Jagutzki, L. Spielberger, J. Ullrich, R. Moshammer and H. Schmidt-Böcking, Physics Reports **330**, 96 (2000).
4. R. Díez Muiño, D. Rolles, F.J. García de Abajo, F. Starrost, W. Schattke, C.S. Fadley and M.A. Van Hove, J. of Electr. Spectr. and Rel. Phenom. **99**, 114 (2001).
5. S.K. Semenov, N.A. Cherepkov, G.H. Fecher and G. Schönhense, Phys. Rev. **A61**, 032704 (2000).
6. N.A. Cherepkov, S.K. Semenov, Y. Hikosaka, K. Ito, S. Motoki and A. Yagishita, Phys. Rev. Lett. **84**, 250 (2000).

This work was supported by the Director, Office of Science, Office of Basic Energy Sciences, Geo-, Bio-, Chemical and Materials Sciences Divisions, of the U.S. Department of Energy under Contract No. DE-AC03-76SF00098.

Principal investigator: Michel A. Van Hove, Advanced Light Source and Materials Sciences Division, Ernest Orlando Lawrence Berkeley National Laboratory. Email: MAVanHove@lbl.gov. Telephone: 510-486-6160.

# Comparison of Magnetic Anisotropy by X-Ray Magnetic Linear Dichroism.

H. Ohldag[1,2,4], S. Maat[3], E. Arenholz[2], A.T. Young[2],
A. Scholl[2], B.A. Gurney[3] and J. Stöhr[1]

[1]Stanford Synchrotron Radiation Laboratory, Stanford University, Stanford, California 94309, USA.
[2]Advanced Light Source, Ernest Orlando Lawrence Berkeley National Laboratory, University of California, Berkeley, California 94720, USA.
[3]IBM Almaden Research Center, San Jose 95120 California, USA.
[4]Institut für Angewandte Physik, Heinrich Heine Universität Düsseldorf, 40225 Düsseldorf, Germany.

## BACKGROUND

Over the last years x-ray magnetic circular dichroism (XMCD) has been established as a technique to reliably determine the direction and the size of the local spin and orbital magnetic moment of a each element in a sample. An interesting property of magnetic systems is the magnetic anisotropy manifested in the observation that spins tend to align parallel to a certain crystal axis to minimize their energy. The origin of the anisotropy lies in the coupling of the electron spin to the orbital moment and thus the crystal lattice. In principal the anisotropy energy can be determined from the difference of the orbital moment measured along different crystal axis. Practically this is rather difficult because of the small size of the orbital moment. Recently experiments employing the x-ray magnetic linear dichroism (XMLD) have been suggested and some very promising first results were published [1,2]. Linear dichroism is not sensitive to a net magnetic moment, but only to the relative orientation between electric field vector and magnetic moment. It can thus be used to determine the energetic difference between two configurations in which the magnetic axes are oriented perpendicular to each other.

We studied the influence of thin films of Ni on the in versus out of plane anisotropy of $CoFe_2O_4$. In all these samples the spins prefer to align parallel to the surface, which is referred to as *in plane anisotropy*. However, we know from hysteresis loops measured using the magneto-optic kerr effect that it is easier to drag the magnetization out of the surface plane if a thin Ni layer is deposited (2nm). Therefore the sample covered with Ni should exhibit a smaller XMLD signal due to the smaller in plane anisotropy. The use of an elliptical undulator beamline offers the possibility to monitor the XMLD signal while rotating the electric field vector continuously from the easy axis of the sample (parallel to the surface) to the magnetic hard axis (perpendicular to the surface)

**RESULTS**

An external field of 2800Oe along the beam direction was applied to fully magnetize the sample. Dichroism spectra were acquired by switching the polarization between 90% plus and minus circular helicity (XMCD) or between fully horizontal and vertical linear polarization (XMLD). Figure 1 shows the comparison between magnetic circular and linear dichroism of Fe 2p in $CoFe_2O_4$. The net XMCD signal has a different sign for $L_3$ and $L_2$ absorption resonance. Sum rules relate the difference in XMCD signal to the net atomic magnetic moment. Another sum rule relates the normalized integral to the orbital moment. Because of the complicated line shape of the iron oxide resonances the accurate determination of the integral is difficult. An alternative is to use the XMLD signal which does not change its sign, because it is not sensitive to the net magnetic moment. In case of XMLD a qualitative determination of the orbital moment is possible only by observing the relative intensity of the two features within each resonance. It reaches a maximum when the anisotropy axis (easy axis) and the electric field are perpendicular to each other.

We now monitored the ratio while rotating the electric field vector away from the surface normal into the surface. Figure 2 shows the result. Both samples show a maximum XMLD signal when the electric field vector is perpendicular to the surface meaning that both samples show an effective in plane anisotropy. Of the electric field vector is rotated towards the sample surface, the XMLD follows the predicted $\cos^2$ dependence [1] for both samples. The absolute value of the XMLD intensity is increased in the sample with the thin Ni layer on top. This demonstrates that indeed the in versus out of plane anisotropy of the $CoFe_2O_4$ is changed by the Ni deposition. The fact that this behavior is also observed in XMLD rules out a pure change in so called *surface anisotropy* by the Ni deposition but that the interaction of the electronic structure of both systems is of importance.

# References


[1] G. van der Laan, *"Magnetic linear X-ray dichroism as a probe of the magnetocrystalline anisotropy"*, Phys. Rev. Lett **82** pp. 640, (1999).

[2] [2] S.S. Dhesi, G. van der Laan, E. Dudzik, A.B. Shick, *"Anisotropic spin-orbit coupling and magnetocrystalline anisotropy in vicinal Co films"*, Phys. Rev. Lett **87**, pp. 067201, (2001)



This work was supported by the Director, Office of Basic Energy Sciences of the U.S. Department of Energy. It was carried out at the Advanced Light Source



Principal investigator: Joachim Stöhr, Stanford Synchrotron Radiation Laboratory, Stanford University, Stanford CA 94309. Email: stohr@slac.stanford.edu

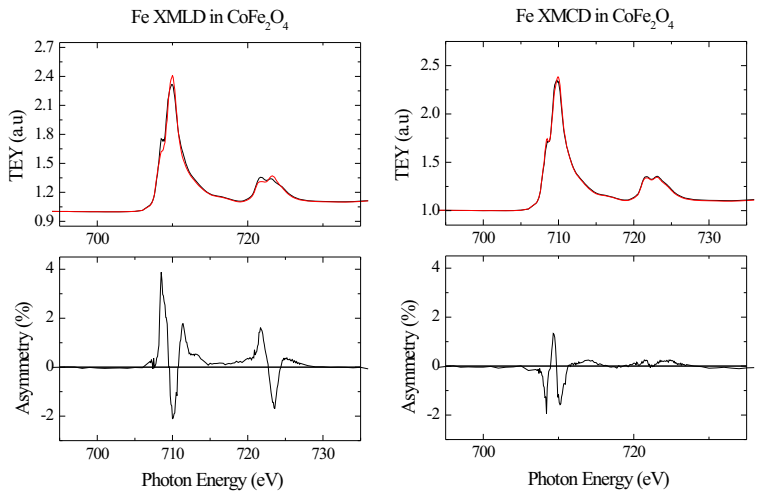


Figure 1: 2p absorption spectra of Fe in $CoFe_2O_4$. The left panel shows XMCD and the right panel the XMLD spectra. The absorption spectra acquired for each polarization are shown on the top. The bottom row displays their difference.

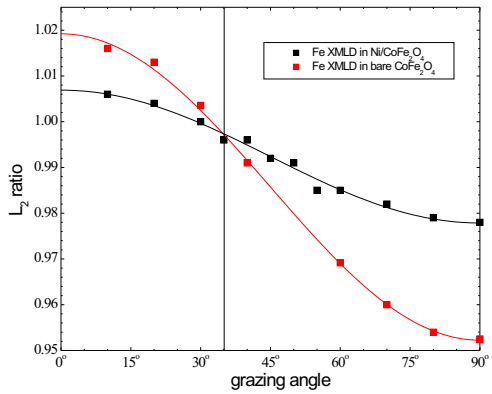


Figure 2: The angular dependence of the XMLD signal in $CoFe_2O_4$ (red) and with a 2nm thin Ni layer (black). The XMLD signal is maximal when the electric field vector is perpendicular to the surface indicating net in plane anisotropy. The absolute amplitude of the XMLD is smaller for the sample covered with Ni, because of the reduced anisotropy. The curves cross at the magic angle, where polarization effects do not play a role.

# Correction of Non-Linearity in Detectors for Electron Spectroscopy

N. Mannella[1,2], S. Marchesini[2], S.-H. Yang[2], B.S. Mun[1,2], A.W. Kay[1,2,#], T. Gresch[2,3], A. Rosenhahn[2] and C.S. Fadley[1,2]

[1]Dept. of Physics, University of California-Davis, Davis, CA 95616
[2]Materials Sciences Division, Lawrence Berkeley National Laboratory, Berkeley, CA 94720
[3]Institute of Physics, University of Zurich, Zurich, Switzerland
[#]Present address: Intel Corporation, Portland, OR

## INTRODUCTION

The intensity levels reached in many third-generation synchrotron radiation experiments on solids have been found to exceed the linear response range of the final detection system involved. In electron spectroscopy, Seah and co-workers have previously discussed methods for detecting such non-linearity, including measurements with laboratory x-ray sources [1]. As a particular case involving synchrotron radiation, non-linearity has been noticed by several groups in using the Gammadata/Scienta electron spectrometers, with this behavior extending even to fairly low countrates [2-8]. For example, prior work on multi-atom resonant photoemission (MARPE) by several groups was strongly affected by this particular non-linearity [3-6]. While data related to the MARPE effect have been corrected for such non-linearities in prior publications [6b,7,8], we have found that other measurements such as the quantitative analysis of complex oxides via core-level intensities can be strongly influenced by this non-linearity, even when the exciting energy is far away from any resonance [9]. Similarly, measurements of relative intensities in angle-resolved valence spectra can also be significantly altered [10]. It is thus of interest to develop accurate and broadly utilizable procedures for correcting for non-linearity with any detection system. Although we will use one spectrometer system as an example, the methodologies discussed here should be useful for many other cases.

## CORRECTION METHODOLOGIES AND EXPERIMENTAL RESULTS

In Figure 1(a), we show broad-range survey spectra from a Cu(110) sample, as excited by Al K$\alpha$ radiation with various power levels and detected by a Scienta SES200 spectrometer and its standard microchannel-plate/phosphor/CCD detection system. Since the high voltage was held constant, this is verified experimentally to lead to x-ray flux being proportional to power [7]. The various spectra have been normalized to one another at the lowest-countrates, just above the valence region. If the detector were linear, all spectra should lie on top of one another, but it is evident that they are not, with factors of up to 4x separating them in the higher intensity regions at lower kinetic energy.

We now consider two methods for correcting for non-linearity in such spectra:

1. Measurement of flat-background reference intensity as a function of incident x-ray flux: In the most obvious method, a flat background region in a spectrum from a sample with a stable surface can simply be measured as a function of incident x-ray flux, with non-linearity then being reflected in any deviation of a plot of measured intensity vs. x-ray flux from a straight line [7]. One might term this a "partial yield" measurement of detector response. This curve can then be fit to a convenient polynomial function such that any non-linearity can be described finally via:

$$I_m(I_t, I_x) = b_0 + b_1 I_t(I_x) + \sum_{n=2}^{n_{max}} b_n I_t(I_x), \tag{1}$$

where $I_m$ = the measured countrate, $I_t$ = the true countrate, $I_x$ = the incident x-ray flux, the $b_n$ are empirical expansion coefficients, and $n_{max}$ is some maximum order chosen to adequately fit the data (roughly 5 in one prior analysis [7]). The coefficient $b_0$ thus represents the dark current in the absence of any excitation, and this will often be negligible, or at least can be simply subtracted from all measurements. The overall counting efficiency $\varepsilon$ is now defined simply as

$$\varepsilon(I_m) = \frac{I_m(I_t, I_x) - b_0}{I_t(I_x)} = b_1 + \sum_{n=2}^{n_{max}} b_n I_t^{n-1}(I_x). \tag{2}$$

Actual measured spectra can now be generally written as vectors $[I_{mi}(E_i)]$ over different energies $E_i$, and can be corrected to yield true spectra $[I_{ti}(E_i)]$ simply by dividing by $\varepsilon$, or

$$I_{ti}(E_i) = [\varepsilon(I_{mi})]^{-1} I_{mi}(E_i) \equiv \delta(I_{mi}) I_{mi}(E_i), \tag{3}$$

where the quantity $\delta(I_{mi})$ is defined by this equation.

Some measured vs. true countrates derived in this way are shown in Figure 1(c), and at minimum a significant quadratic correction term is evident. This procedure has been used in a prior analysis of detector non-linearity by Kay and co-workers [7,8], and it is found to yield excellent correction for such effects in the Scienta system, including the MARPE data discussed previously.

2. Analysis of broad-scan survey spectra at different incident x-ray fluxes:

Consider a set of $N$ survey spectra $I_{mi}^j(I_x^j, E_j)$ measured on the same sample, with incident fluxes $j = 1, 2, \ldots, N$, as illustrated shown in Figure 1(a). The intensities here span a range of approximately 40x, thus sampling the detector response very fully. We further assume that the true countrate $I_{ti}^j$ (minus dark current as needed) for a given flux $I_x^j$, and energy $E_i$, can be expressed via a simple proportionality to flux, and that the true spectra can also be described by another power series in the measured spectra, as

$$I_{ti}^j(I_x^j, E_i) = I_x^j I_0(E_i) = \sum_{k=1}^{P} a_i I_{mi}^k(E_i), \tag{4}$$

where $I_0(E_i)$ = the true spectral shape in energy, $j = 1, 2, \ldots, N$; $i = 1, 2, \ldots, M$ = no. of channels in energy, and $P$ is the maximum order of the polynomial needed to adequately describe the data (roughly 9 as a conservative number). Further assuming that the detector is linear at very low count rates such that, and then substituting for $I_{ti}^1$ and rearranging, permits expressing the data for all N spectra as:

$$\underbrace{-\left[\frac{I_{mi}(I_x^1, E_i)}{I_x^1} - \frac{I_{mi}(I_x^j, E_i)}{I_x^j}\right]}_{=\mathbf{B}} = \sum_{k=2}^{P} \underbrace{\left[\frac{I_{mi}^k(I_x^1, E_i)}{I_x^1} - \frac{I_{mi}^k(I_x^j, E_i)}{I_x^j}\right]}_{=\mathbf{M}} \underbrace{a_i}_{=\mathbf{A}}. \tag{5}$$

In matrix form, $\mathbf{B}$ is an $(N-1)\bullet M$ long column vector, $\mathbf{M}$ an $(N-1)\bullet M$ by $(P-1)$ matrix, and $\mathbf{A}$ a $(P-1)$ long column vector. Eq. (5) is an over-determined system of linear equations and can be solved for the maximum likelihood $a_i$'s in $\mathbf{A}$ by finding the minimum of $|\mathbf{B} - \mathbf{MA}|^2$, *i.e.* by solving for $0 = \nabla_A|\mathbf{B}-\mathbf{MA}|^2 = 2\mathbf{M}^\mathbf{T}\mathbf{M} - 2\mathbf{M}^\mathbf{T}\mathbf{B}$ (superscript $\mathbf{T}$ = transpose). The polynomial coefficients in can by obtained by a standard "LU" decomposition [11] or simply by matrix inversion:

$$\mathbf{A} = (\mathbf{M}^\mathbf{T}\mathbf{M})^{-1}\mathbf{M}^\mathbf{T}\mathbf{B}. \tag{6}$$

where $\left(\mathbf{M}^{\mathrm{T}}\mathbf{M}\right)$ is a small $\left(P-1\right)$ by $\left(P-1\right)$ matrix. For better numerical precision in the matrix inversion, the measured counts should vary from 0 to 1, which can be achieved by trivial normalization.

Some results obtained with both methods are shown in Figure 1(d), where the true counts are plotted as a function of measured counts, and essentially identical results for the curve are found from both methods. Finally, in Figure 1(b), we show the same spectra as Figure 1(a), but with the correction applied: it is clear that all normalized spectra for different fluxes coincide to a high accuracy, thus permitting quantitative spectroscopy to be performed with this detector.

## CONCLUSIONS

In summary, we have presented two distinct methods for correcting for non-linearity in detection systems, and demonstrated their validity for the specific case of the Scienta SES 200 spectrometer. Applications to this and other spectrometer systems for electrons and soft x-rays should be possible.

## REFERENCES


1. (a) M.P. Seah, M. Tosa, Surf. Interface. Anal. **18** (1992) 240; (b) M.P. Seah, I.S. Gilmore, S.J. Spencer, J. Electron Spectrosc. **104** (1999) 73-89.
2. M.P. Seah, M.Tosa, Surf. Interface. Anal. 18 (1992) 240; (b) M.P. Seah, I.S. Gilmore, S.J. Spencer, J. Electron Spectrosc. 104 (1999) 73-89.
3. A. Kay, E. Arenholz, B.S. Mun, F.J. Garcia de Abajo, C.S. Fadley, R. Denecke, Z. Hussain, and M.A. Van Hove, *Science* **281**, 679(1998).
4. E. Arenholz, A.W. Kay, C.S. Fadley, M.M. Grush, T.A. Callcott, D.L. Ederer, C. Heske, and Z. Hussain, *Phys. Rev. B* **61**, 7183 (2000).
5. A. Kikas, E. Nommiste, R. Ruus, A. Saar, and I. Martinson, Sol. St. Commun. **115**, 275 (2000).
6. (a) M.G. Garnier, N. Witkowski, R. Denecke, D. Nordlund, A. Nilsson, M. Nagasono, and N. Mårtensson, and A. Föhlisch, Maxlab Annual Report for 1999 and private communication correcting this data; (b) D. Nordlund, M.G. Garnier, N. Witkowski, R. Denecke, A. Nilsson, M. Nagasono, N. Martensson, A. Fohlisch, Phys. Rev. B 63, 121402 (2001).
7. A.W. Kay, Ph.D. dissertation (University of California-Davis, September, 2000), Chapters 4 and 5.
8. A.W. Kay, F.J. Garcia de Abajo, S.H. Yang, E. Arenholz, B.S. Mun, M.A. Van Hove, Z. Hussain, and C.S. Fadley, Physical Review B **63**, 5119 (2001), and Proceedings of the Eighth International Conference on Electronic Spectroscopy and Structure, J. Electron Spectrosc. **114**, 1179 (2001).
9. N. Mannella et al., private communication.
10. D. Dessau and Y. Chuang, private communication.
11. W. H. Press, S. A. Teukolsky, W. T. Vetterling, B. P. Flannery, "Numerical Recipes in C: The Art of Scientific Computing", Cambridge University Press, New York, 1992, pp. 43-50.



This work was supported by the U.S. Department of Energy, Office of Science, Office of Basic Energy Sciences, Materials Sciences Division, under Contract No. DE-AC03-76SF00098..



Principal investigator: Norman Mannella, Department of Physics UC Davis, and Materials Sciences Division, Lawrence Berkeley National Laboratory. Email: norman@electron.lbl.gov. Telephone: 510-486-5446

Figure 1. (a) Survey spectra from a Cu(110) sample, obtained with AlKα excitation at various x-ray powers and constant voltage, normalized to be equal at the lowest countrates near zero binding energy. (b) Survey spectra for the four lowest power settings after non-linearity correction. (c) Plot of true countrate vs. measured countrate, as derived from Method 1. Countrates expressed in Hz per pixel in the CCD camera [7,8]. (d) Plot of measured countrate vs. true countrate as derived from both Methods 1 and 2.

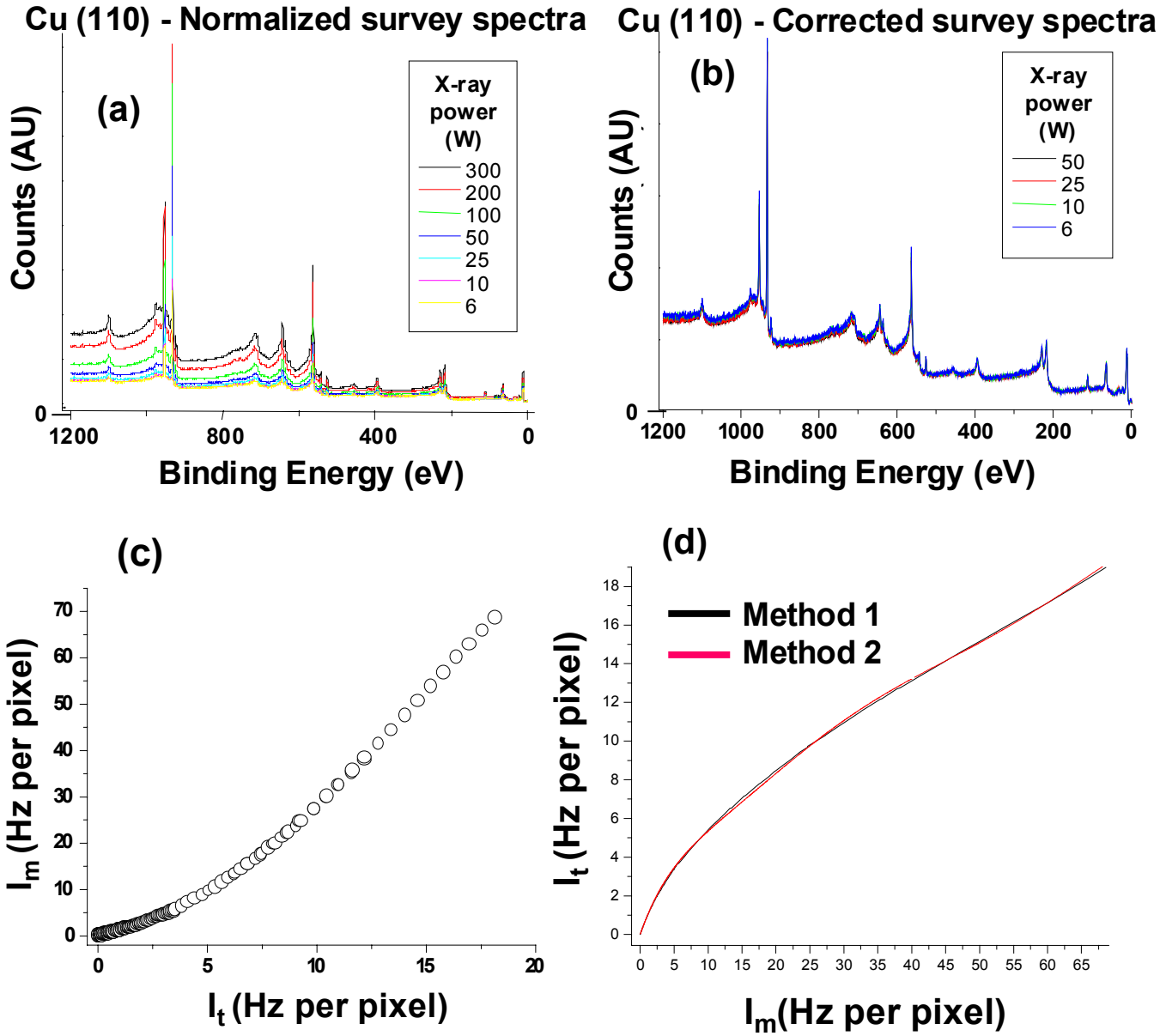

# Development of a GHz-Rate Detector for Synchrotron Radiation Research

B. Turko[3], M. Press[3], A.W. Kay[1,2,#], M. West[1,3], J.E. Katz[3], H. Spieler[5], Z. Hussain[4], C.S. Fadley[1,2], B. Ludewigt[3], J.-M. Bussat[3], P. Denes[3], H. von der Lippe[3], G. Meddeler[3], G. Zizka[3], G, Lebedev [4], M. Mellon[6], T. Wiell[7]

[1]Materials Sciences Division, LBNL, Berkeley, CA 94720
[2]Dept. of Physics, UC Davis, Davis, CA 95616
[3]Engineering Sciences Division, LBNL
[4]Advanced Light Source, LBNL, Berkeley, CA 94720
[5]Physics Division, LBNL, Berkeley, CA 94720
[6]Quantar Technology, Santa Cruz, CA
[7]Gammadata/Scienta AB, Uppsala, Sweden
[#]Present address: Intel Corporation, Portland, OR

## INTRODUCTION

It has by now become obvious that the brightness of third-generation synchrotron radiation sources often exceeds the capabilities of the end-station detector systems to adequately handle the electron or photon fluxes resulting from a given experiment, thus preventing both the fullest utilization of the radiation and the carrying out of certain new types of experiments readily, if at all. Detector non-linearity is one problem that has been encountered [1], but there are many other examples for which beamline or spectrometer throughput must be decreased to prevent high countrate saturation, or the number of energy or angular channels that can be counted simultaneously severely limits a given experiment [2]. In recognition of this, a national-level initiative in detector development has been proposed by the multi-institutional "DetectorSync" group [2].

As a first example of what can be accomplished with advanced detector technology, a project to develop an ultrahigh-speed one-dimensional detector for electrons and vuv/x-ray photons is underway at the ALS.

## DESIGN PHILOSOPHY AND FIRST TEST RESULTS

This project takes advantage of unique expertise at LBNL for detector development in high-energy and nuclear physics, and involves the custom design and fabrication of application-specific integrated circuits (ASICs). The final goal is a 768-channel detector with 50 micron spacing between channels and a maximum linear countrate per channel of over 2 megaherz. The overall countrate will thus be in the 2 GHz range, and approximately 100 times faster than any other present one-dimensional or two-dimensional detector, with significantly improved spatial resolution as well compared to other existing detectors. First applications will be in electron spectroscopy, but others in x-ray absorption and x-ray emission spectroscopy are expected to follow.

A first prototype of this detector is shown in Fig. 1(a). Based on 12 pairs of 64-channel ASICs (an existing high-energy preamplifier chip (SDC) and a specially-designed buffered counter (DBC)), this detector has already demonstrated the ability to take spectra in a Scienta electron spectrometer located at the ALS (Fig. 2(a)), to resolve channels with a FWHM of 75 microns (Fig. 2(b)), and to count linearly at up to 1.0 GHz overall (Fig. 2(c)) [3].

Based on this experience, a next-generation detector with significant improvements in all elements from power supplies to ASICs to data acquisition is presently under development, with an expected completion date of late 2002. This will use 6 pairs of 128-channel ASICs (a newer high-energy preamplifier chip (CAFÉ-M) and a specially-designed buffer counter (BMC)), with optical coupling between detector and control/counting electronics to minimize noise and transients. The completion date for this project is estimated to be late 2002.

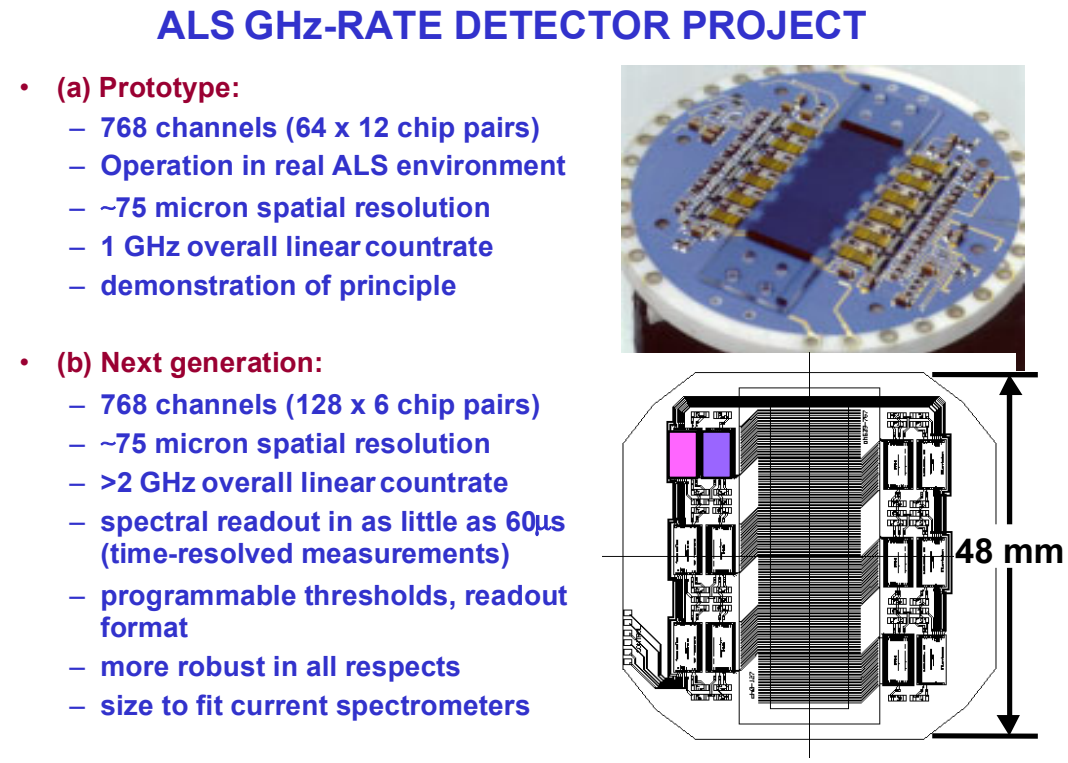


Figure 1--(a) Basic characteristics of the prototype GHz-rate detector developed as the first stage of this project, together with a photo of the ceramic substrate with 12 preamp-plus-counter chipsets mounted on it. The microchannel plates are not yet installed. (b) Basic characteristics of the next-generation detection now being designed and fabricated, together with a layout of its 6 chipsets and an indication of its size.

## CONCLUSIONS

A prototype one-dimensional electron and photon detector operating linearly up to the GHz countrate level and with a resolution of 75 microns over 768 channels has been successfully developed and tested. An improved version of this detector is under development, with the same resolution and number of channels, but improved performance, programmability, and robustness in general user environments relative to the prototype. The next-generation detector should find use in several areas of synchrotron radiation research.

## REFERENCES

[1] A.W. Kay, F.J. Garcia de Abajo, S.-H. Yang, E. Arenholz, B.S. Mun, N. Mannella, Z. Hussain, M.A. Van Hove, and C.S. Fadley, Phys. Rev. B 63, 115119 (2001); D. Nordlund, M.G. Garnier, N. Witkowski, R. Denecke, A. Nilsson, M. Nagasono, N. Martensson, A. Fohlisch, Phys. Rev. B 63, 121402 (2001); and abstract in the 2001 Compendium by N. Mannella et al.

[2] Local participants in the DetectorSync initiative include A. Thompson, H.A. Padmore, and C.S. Fadley, and the group's website is at--http://www-esg.lbl.gov/esg/meetings/detectorsync/index.html, with a more detailed white paper on detector needs also downloadable from this source.
[3] A.W. Kay, Ph.D. thesis (University of California, Davis, September, 2000), LBNL report 46885, and to be published.

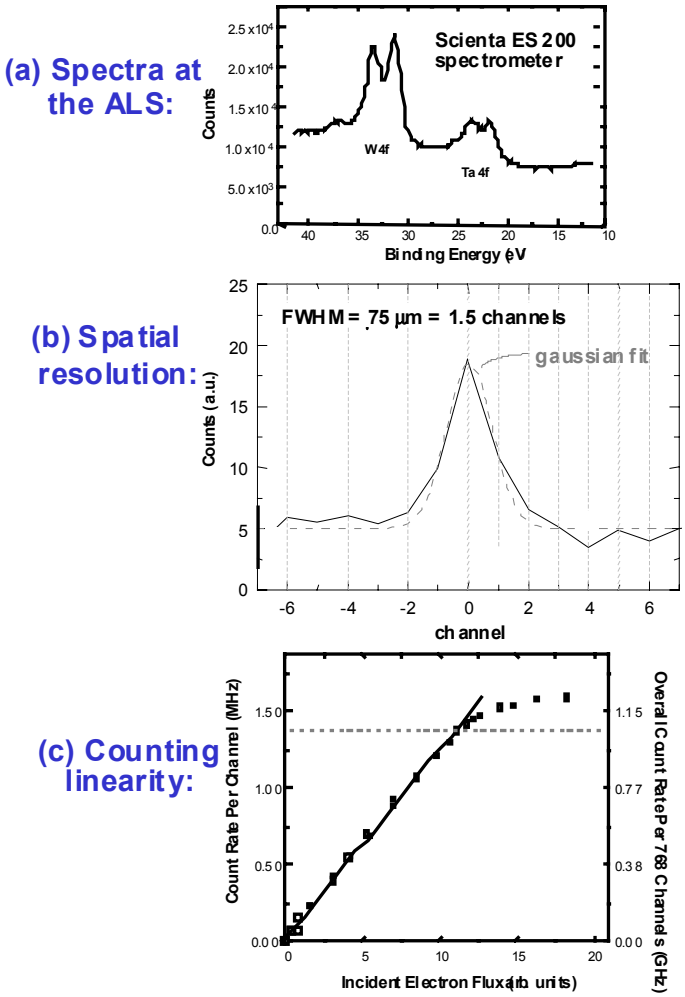


Figure 2--Test data from the first prototype detector shown in Fig. 1(a). (a) Test spectra obtained with the detector mounted in a Scienta SES 200 spectrometer at ALS beamline 9.3.2. (b) Spatial resolution determination via a collimated electron beam source. Each channel is 50 microns. (c) Counting linearity per channel (ledt scale) and over all channels (right scale) as determined with an electron gun.

This work was supported by the U.S. Department of Energy, Office of Science, Office of Basic Energy Sciences, Materials Sciences Division, under Contract No. DE-AC03-76SF00098..

Principal investigator: Charles S. Fadley, Department of Physics UC Davis, and Materials Sciences Division, Lawrence Berkeley National Laboratory. Email: fadley@lbl.gov. Telephone: 510-486-5774

# Magnetic Circular Dichroism in the X-ray Absorption Spectra of the CMR Compound, $Yb_{14}MnSb_{11}$

A. P. Holm[1]; S. M. Kauzlarich[1]; S. A. Morton[2]; G. D. Waddill[3];
W. E. Pickett[4]; J. G. Tobin[2]

[1]Department of Chemistry, University of California, Davis, CA 95616.
[2]Lawrence Livermore National Laboratory, Livermore, CA 94550.
[3]Department of Physics, University of Missouri-Rolla, Rolla, MO 65401-0249.
[4]Department of Physics, University of California, Davis, CA 95616.

This work is part of ongoing investigations into the magnetic and electronic properties of the rare-earth transition metal Zintl phases $A_{14}MnPn_{11}$ (A = Eu, Yb; Pn = Sb, Bi) at the Advanced Light Source. We have recently obtained exciting new results from X-ray magnetic circular dichroism (XMCD) investigations of the $Yb_{14}MnSb_{11}$ system. Specifically, we have used XMCD as an element specific probe into the nature of the magnetic moment in this system with the intention of exploring the proposed half-metallic nature of this compound and its related substitutional analogues. Our XMCD measurements indicate that $Yb_{14}MnSb_{11}$ is a half-metallic ferromagnet, and we have submitted our results for publication to Physical Review Letters.

The term half-metallic ferromagnet arises from theoretical predictions made by R.A. de Groot et al based on band structure calculations of the ferromagnetic Heusler alloy NiMnSb.[1] These calculations proposed a new phase of matter that displays separate electronic properties for majority-spin and minority-spin electrons. Specifically, one electron spin population is metallic and the other is insulating. Such a material, (possessing 100% spin polarization of the conduction electron) would hold significant technological potential as a single-spin electron source for spintronic devices, data storage applications, and high efficiency magnetic sensors.[2]

The materials we are studying are new compounds that belong to a class of materials called transition-metal Zintl phases. These compounds are isostructural to $Ca_{14}AlSb_{11}$ and crystallize in the tetragonal space group $I4_1/acd$ (Z = 8). The $Yb_{14}MnSb_{11}$, $Yb_{14}MnBi_{11}$ and $Eu_{14}MnSb_{11}$ analogues are each reported to order ferromagnetically at 56 K, 58 K and 28 K, and 92 K, respectively.[3-6] $Eu_{14}MnBi_{11}$ is an antiferromagnet with a Néel transition at $T_N$ = 32 K.[6] Each of these materials exhibits a large resistance drop associated with their unique magnetic ordering temperature. This behavior is attributed to colossal magnetoresistance effects, and could help support the proposal made by Pickett and Singh of a correlation between half-metallicity and colossal magnetoresistance.[7] These systems are ideal for investigations into the links between magneto-resistance, magnetic moment and half-metallic behavior.

The ability to perform X-ray magnetic circular dichroism experiments on the EPU has allowed us to probe the dichroic characteristics of Mn and Sb in the $Yb_{14}MnSb_{11}$

system during experiments recently performed on beamline 4.0 of the ALS. Figure 1 shows the results from XMCD experiments on the Mn $L_{23}$, Sb $M_{45}$, and Yb $N_{45}$ edges of $Yb_{14}MnSb_{11}$. A dramatic dichroism effect is shown in the Mn $L_{23}$ region which is confined to one sub-component of the Mn edge and closely matches theoretical models for $Mn^{2+}$, $d^5$ dichroism (Figure 1d). The difference in intensity upon change of helicity is greater than 30%, and is strong evidence of a significant moment being present on the Mn. In contrast, no dichroism was observed in the Yb edges, but a small antialigned moment is present in the Sb $M_{45}$ edges as shown on the left side of Figure 1. This result is surprising because initial models predicted that dichroism would be restricted to the Mn $L_{23}$ region (with no dichroism in the Sb $M_{45}$ region) and that it would be $Mn^{3+}$, $d^4$ like in character. However, an ongoing collaboration with theoretical groups in the physics departments of the University of California, Davis and the University of Illinois, Urbana to model the Ca and Ba analogues of this structure type has now produced calculated results consistent with our experimental observations of how the Sb behaves in this system. They argue that the Mn should be in a 2+, $d^5$ configuration, and the $Sb_4$ cage surrounding the Mn should have a hole antialigned to the Mn moment giving a total moment of ~4 $\mu_B$/ formula unit. Our experimental results are consistent with these new theoretical results, and in addition, these comparisons of data with theoretical calculations and SQUID magnetometry measurements confirm that $Yb_{14}MnSb_{11}$ is indeed a half-metallic ferromagnet.[8-10]

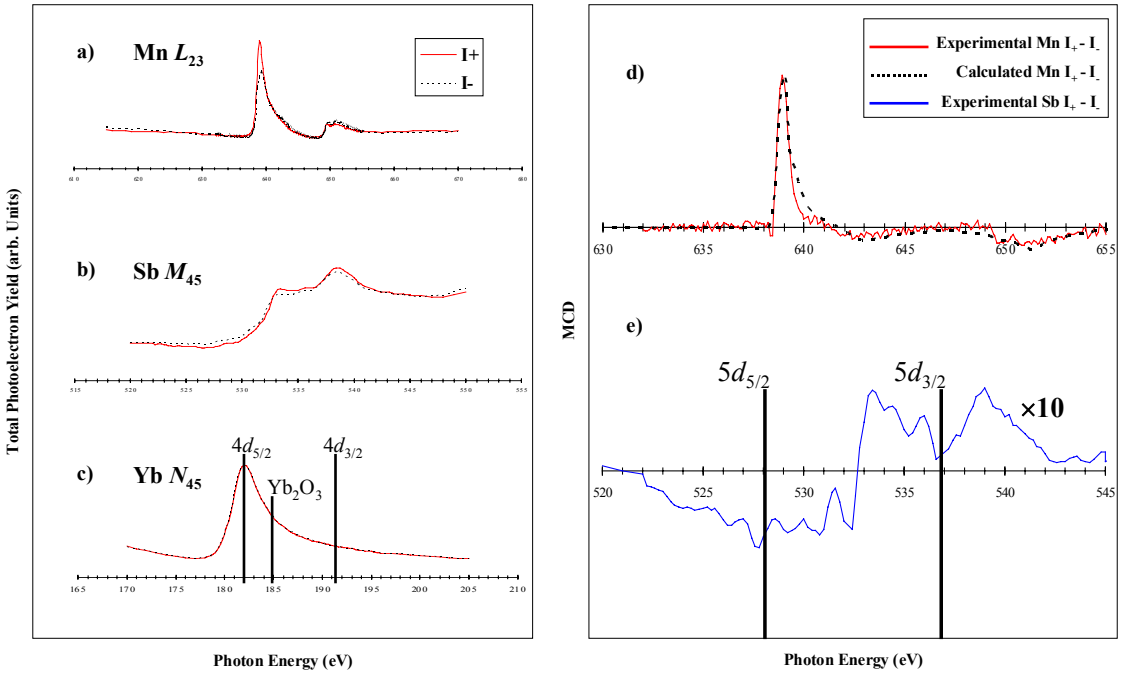


Fig. 1. The raw absorption spectra at plus and minus light polarization for a) Mn $L_{23}$, b) Sb $M_{45}$, and c) Yb $N_{45}$ are shown on the left. The MCD spectra for d) the experimental Mn $L_{23}$ denoted by a solid red line and the calculated $Mn^{2+}$, $d^5$ $L_{23}$ denoted by a dashed black line, and e) the experimental Sb $M_{45}$ denoted by a solid blue line.[10]

**References:**


1. de Groot, R. A.; Mueller, F. M.; van Engen, P. G.; Buschow, K. H. J. *Physical Review Letters* **1983**, *50*, 2024 -2027.
2. Prinz, G. A. *Science* **1998**, *282*, 1660 - 1663.
3. Chan, J. Y.; Kauzlarich, S. M.; Klavins, P.; Shelton, R. N.; Webb, D. J. *Chemistry of Materials* **1997**, *9*, 3132-3135.
4. Chan, J. Y.; Olmstead, M. M.; Kauzlarich, S. M.; Webb, D. J. *Chemistry of Materials* **1997**, *10*, 3583 - 3588.
5. Chan, J. Y.; Wang, M. E.; Rehr, A.; Kauzlarich, S. M.; Webb, D. J. *Chemistry of Materials.* **1997**, *9*, 2131 - 2138.
6. Chan, J. Y.; Kauzlarich, S. M.; Klavins, P.; Shelton, R. N.; Webb, D. J. *Physical Review B* **1998**, *57*, 8103 - 8106.
7. Pickett, W. E.; Singh, D. J. *Physical Review B* **1996**, *53*, 1146 - 1160.
8. Sánchez-Portal, D.; Martin, R. M.; Kauzlarich, S. M.; Pickett, W. E. *Physical Review B* **2001**, *Submitted September 31*.
9. van der Laan, G.; Thole, B. T. *Physical Review B* **1991**, *43*, 13401-13411.
10. Holm, A. P.; Kauzlarich, S. M.; Morton, S. A.; Waddill, G. D.; Pickett, W. E.; Tobin, J. G. *Physical Review Letters* **2001**, *Submitted November 26*.



This work was supported by the Director, Office of Energy Research, Office of Basic Energy Sciences, Materials Science Division, of the U.S. Department of Energy under Contract No. # R5-32633.A02. This work was performed under the auspices of the U.S Department of Energy by Lawrence Livermore National Laboratory under contract no. W-7405-Eng-48.



Principal Investigator: Susan M. Kauzlarich, Department of Chemistry, University of California Davis, California 95616. Phone: (530)752-4756 fax: (530)752-8995 Email: smkauzlarich@ucdavis.edu

# Magnetic Properties of $Fe_3O_4$ Films Grown by Epitaxial Electrodeposition on the Low Index Planes of Gold

J.A. Switzer[1], T.A. Sorenson[1], S.A. Morton[2], and G.D. Waddill[2]
[1]Department of Chemistry and Graduate Center for Materials Research
[2]Department of Physics and Graduate Center for Materials Research
University of Missouri-Rolla, Rolla, Missouri 65409-1170, USA

Spin-dependent charge transport is currently receiving a lot of attention due to potential applications in giant magnetoresistive (GMR) devices such as magnetic field sensors, magnetoresistive random access memories (MRAM), read heads, and galvanic isolators.[1,2] These devices require a source of spin-polarized electrons. Magnetite, $Fe_3O_4$, is a promising source of spin-polarized carriers, because density-functional theory spin-resolved density of states calculations have suggested that electrons at the Fermi level are -100% spin polarized.[3,4] Magnetite is a mixed-valence 3d transition metal oxide that has an inverse spinel structure (space group *Fd3m*) with a lattice constant of 0.8397 nm. The tetrahedral sites of the spinel structure are entirely occupied by $Fe^{3+}$, whereas the octahedral sites are occupied half by $Fe^{2+}$ and half by $Fe^{3+}$. $Fe_3O_4$ undergoes a metal-to-insulator Verwey transition at 120 K and the Curie temperature of magnetite is 860 K. Recently, GMR effects greater than 500% have been reported at room temperature for $Fe_3O_4$ nanocontacts.[5]

We have electrodeposited galvanostatically epitaxial $Fe_3O_4$ films on Au(111), a system with a 3% lattice mismatch.[6] These films are ~0.5 μm thick and have a (111) orientation. X-ray diffraction and SEM results establish that the magnetite films consist of twinned domains rotated by 180° with respect to each other. For the spin-polarized photoemission measurements a magnetic field from an *in situ* electromagnet is applied to the sample either in the plane of the sample or perpendicular to that plane. The field is then removed and the photoemission measurements are performed in remanence. The spin-resolved measurements were done at Beamline 7.0.1 with the spin-resolved endstation.[7] The energy of the excitation beam was ~ 160 eV. Emitted photoelectrons were collected and filtered by a PHI 10-360 SCA hemispherical electron energy analyzer and then passed into a micro-Mott detector to resolve the electron spins. The total energy resolution for the spin resolved measurements was ~0.5 eV. Finally we have measured Fe L edge and O K edge XAS as well as Fe MXCD for these samples at Beamline 4.0. For the MXCD measurements, the sample was magnetized *in situ* and the measurements were made in remanance. All measurements were made at room temperature. Prior to the photoemission, XAS, and MXCD measurements the samples are briefly sputtered and then annealed in an oxygen environment. This produces LEED patterns consistent with the presence of rotationally twinned $Fe_3O_4$(111), but the films are rather poorly ordered. Photoemission always observes a trace amount of surface carbon.

The Fe L edge and O K edge XAS are shown in Figs. 1 and 2 respectively. In Fig. 3 we show the Fe L edge MXCD. These results are virtually indistinguishable from results reported by Kim *et al*. for a bulk magnetite sample.[8] Figs. 4 and 5 show the spin-resolved photoemission results for these samples. The polarization at the Fermi level is approximately – 40% with a change in the sign of the polarization observed at ~1 eV binding energy. The reasons for the observed deviation from the predicted value of –100% is not known. There are two recent repots for *in situ* prepared $Fe_3O_4$ films that report either – 50%[9] or – 80%[10] spin-polarization. The first result

is attributed to correlation effects that set an upper limit on the spin-polarization of – 67%[11] while the latter is regarded as evidence for half-metallic behavior. The discrepancy between these various results requires further investigation.

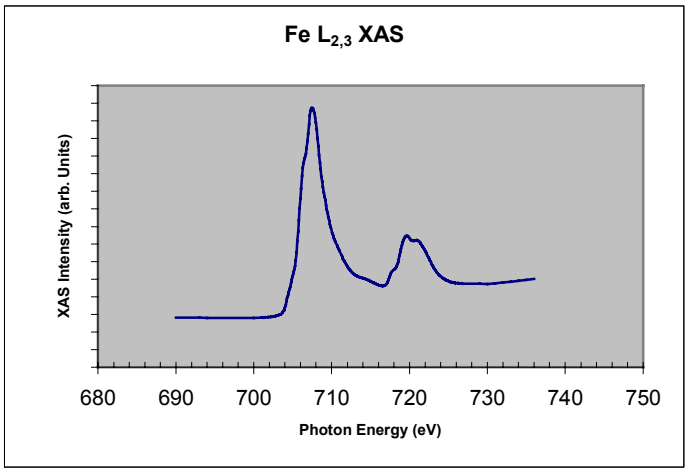


Figure 1. Fe L edge x-ray absorption for thick magnetite film on Au(111).

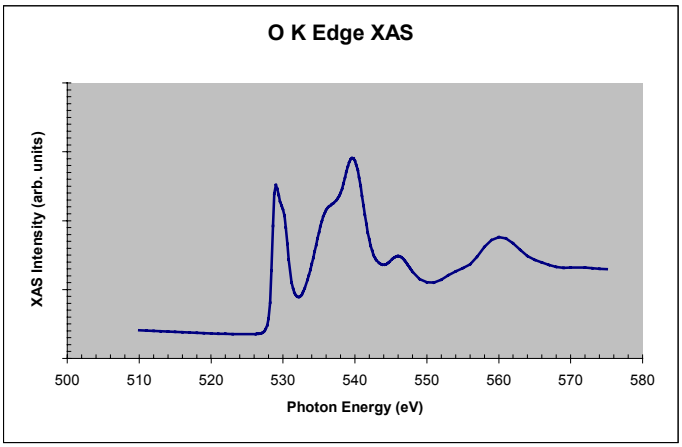


Figure 2. O K edge x-ray absorption for thick magnetite film on Au(111).

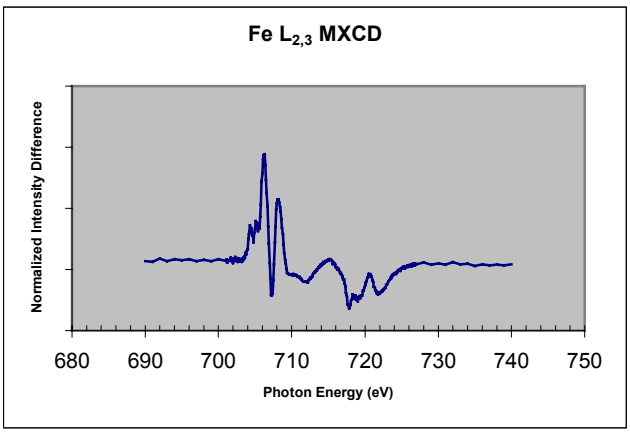


Figure 3. Fe L edge magnetic x-ray circular dichroism for thick magnetite film on Au(111).

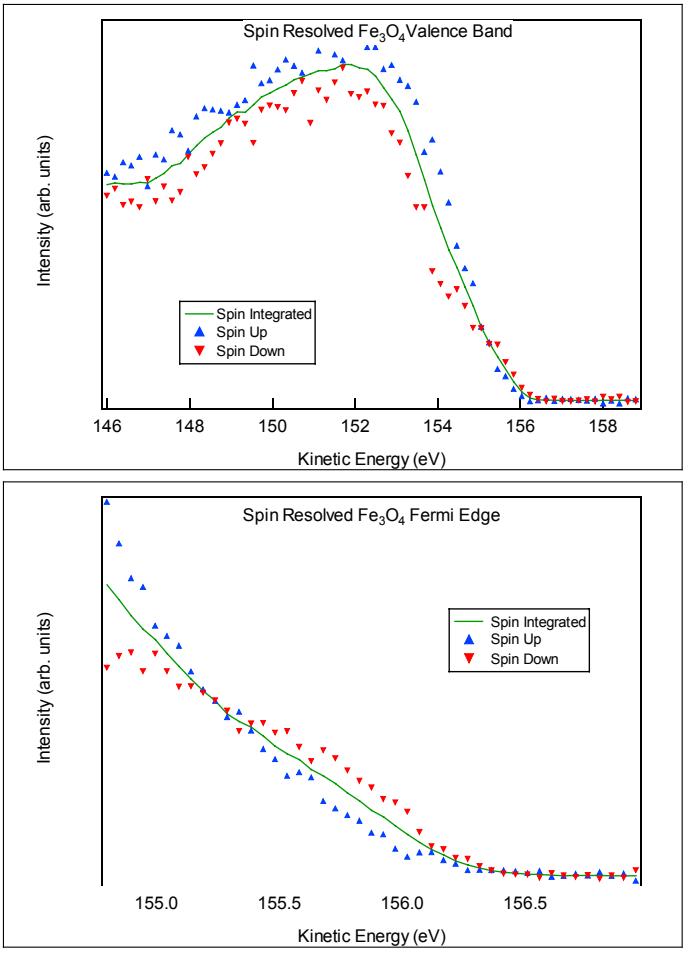


Figure 4. Spin-resolved valence band and Fermi edge for magnetite on Au(111).

## REFERENCES


1. G.A. Prinz, Science **282**, 1660 (1998).
2. S.A. Wolf, D.D. Awschalom, R.A. Buhrman, J.M. Daughton, S. von Molnar, M.L. Roukes, A.Y. Chtchelkanova, D.M. Treger, Science **294**, 1488 (2001).
3. Z. Zhang and S. Satpathy, Phys. Rev. B **44**, 13319 (1991).
4. V.I. Anisimov, I.S. Elfimov, N. Hamada, and K. Terakura, Phys. Rev. B **54**, 4387 (1996).
5. J.J. Versluijs, M.A. Bari, and J.M.D. Coey, Phys. Rev. Lett. **87**, 026601 (2001).
6. M.P. Nikiforov, A. Vertegel, M.G. Shumsky, and J.A. Switzer, Adv. Mater. **12**, 1351 (2000).
7. J.G. Tobin, P.J. Bedrossian, T.R. Cummings, G.D. Waddill, S. Mishra, P. Larson, R. Negri, E. Peterson, P. Boyd, and R. Gunion, MRS Symp. Proc. **524**, 185 (1998).
8. H.J. Kim et al., Phys. Rev. B61, 15284 (2000).
9. D.J. Huang, L.H. Tjeng, J. Chen, C.F. Chang, W.P. Wu, A.D. rata, T. Hibma, S.C. Chung, S.-G. Shyu, C.-C. Wu, and C.T. Chen, Surf. Rev. Lett. (in press).
10. Y.S. Dedkov, U. Rudiger, and G. Guntherodt, Phys. Rev. B **65**, 064417 (2002).
11. S.F Alvarado, W. Eib, F. Meier, D.T. Pierce, K. Sattler, H.C. Siegmann, J.P. Remeika, Phys. Rev. Lett. **34**, 319 (1975).



The National Science Foundation (CHE 9816484, DMR 0071365, and DMR 0076338) and the Foundation for Chemical Research are gratefully acknowledged for financial support of this work.



Principal investigator: Dan Waddill, Department of Physics and Graduate Center for Materials Research, University of Missouri-Rolla. Telephone: 573-341-4797. Email: waddill@umr.edu.

# Magnetic Properties of Uncompensated Spins in Co/NiO

H. Ohldag[1,2,5], F. Nolting[3], E. Arenholz[2], A. Scholl[2],
A.T. Young[2], S. Maat[4], M. Carey[4] and J. Stöhr[1]

[1]Stanford Synchrotron Radiation Laboratory, Stanford University, Stanford, California 94309, USA.
[2]Advanced Light Source, Ernest Orlando Lawrence Berkeley National Laboratory, University of California, Berkeley, California 94720, USA.
[3]Swiss Light Source, Paul Scherrer Institut, 5232 Villingen, Switzerland.
[4]IBM Almaden Research Center, San Jose 95120 California, USA.
[5]Institut für Angewandte Physik, Heinrich Heine Universität Düsseldorf, 40225 Düsseldorf, Germany.

## BACKGROUND

The investigation of magnetic multilayers is an active research area, driven by the interesting physics associated with such structures and their application in the magnetic storage industry. While the interface itself is supposed to dominate the magnetic behavior of the entire system, the identification and characterization of its magnetic properties remains an experimental challenge. A prominent example is the so called exchange bias effect, which is the directional coupling between the spins in an antiferromagnet and those in an adjacent ferromagnet, for a review see [1]. An important parameter in modelling the exchange bias effect are possible uncompensated spins in the antiferromagnet. Recently, we demonstrated the existence of uncompensated Ni spins in the Co/NiO system with XMCD [2] and PEEM [3] measurements and related them to an oxidation/reduction effect at the interface. Here we present hysteresis loops of exchange biased Co/NiO multilayer measured with X-ray absorption spectroscopy (XAS). The experiment was performed at the elliptically polarizing undulator beamline 4.0.2 of the Advanced Light Source, USA.

## RESULTS

The sample studied was a multilayer of 3 nm Co and 50 nm NiO grown on Si. The surface (Co on top) was capped with a 1.5 nm Ru layer to prevent its oxidation. The easy axis of the Co layer was in the plane of the sample and an exchange bias field of 175 Oe was obtained. The XAS spectra were measured in the absorption mode by measuring the sample current. The sample was mounted in grazing incidence in the gap

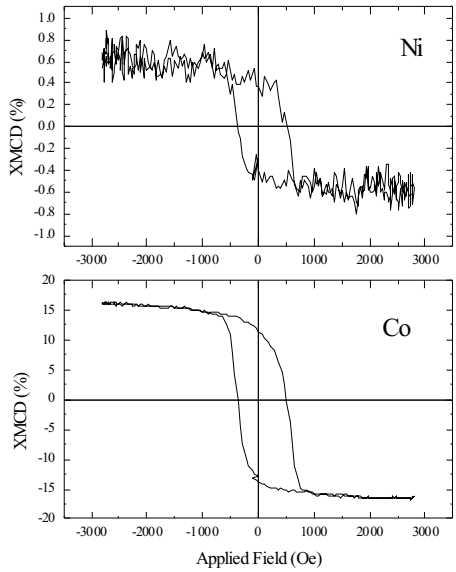


Figure 1: Hysteresis loops of ferromagnetic Co and interfacial ferromagnetic Ni. The Ni signal arises from an equivalent of 0.5ML buried below 4nm of Co and Ru. The loops show no qualitative differences within the error of the experiment.

of an electromagnet, which can switch a magnetic field up to 3000 Oe with 1 Hz and has the magnetic field along the polarization vector of the circularly polarized light. The hysteresis loop for Ni is measured as follow. The magnetic field is varied from -3000 Oe to +3000 Oe and back in 50 Oe steps. At each magnetic field the absorption signal at the $L_3$ and $L_2$ edge for a fixed polarization is measured. Next the measurement is repeated with opposite polarization. The hysteresis loop is calculated by taking the ratio of both polarizations for each edge and then calculating the difference between $L_3$ and $L_2$ loop. The hysteresis loop for Co is obtained in the same way.

Within the experimental error there are no differences between the Co and the Ni loop. A final decision whether all interfacial spins rotate in the external field together with the Co spins or a small fraction of them remains *pinned* to introduce the unidirectional anisotropy cannot be made. This is due to the fact that the vertical position of the loops is slightly influenced by experimental factors and the absolute zero line has to be determined by a reference measurement with an unbiased sample. However we estimate the amount of pinned moments to be less than 20%. A more accurate investigation is currently underway. Nevertheless the determination of element specific hysteresis loops with excellent depth sensitivity and the ability to pick up the magnetic signal arising from small amount of buried material is a promising first result.

# References

[1] J. Noguès and I.K. Schuller, J. Magn. Magn. Mater. 192, 203 (1999).

[2] F. Nolting, E. Arenholz, A.T. Young, A. Scholl, H. Ohldag, and J. Stöhr, ALS Compendium, 2000, LBNL publication, 47838.

[3] H. Ohldag, T. J. Regan, J. Stöhr, A. Scholl, F. Nolting, J. Lüning, C. Stamm, S. Anders, and R. L. White, Phys. Rev. Lett. 87, 247201 (2001).

This work was supported by the Director, Office of Basic Energy Sciences of the U.S. Department of Energy. It was carried out at the Advanced Light Source

Principal investigator: Joachim Stöhr, Stanford Synchrotron Radiation Laboratory, Stanford University, Stanford CA 94309. Email: stohr@slac.stanford.edu

# Mechanisms of Photo Double Ionization of Helium by 530 eV Photons

A. Knapp[1], A. Kheifets[2], I. Bray[3], Th. Weber[1], A. L. Landers[4], S. Schössler[1], T. Jahnke[1], J. Nickles[1], S. Kammer[1], O. Jagutzki[1], L. Ph. Schmidt[1], T. Osipov[5], J. Rösch[1,6], M. H. Prior[6], H. Schmidt-Böcking[1], C. L. Cocke[5] and R. Dörner[1]

[1] Institut für Kernphysik, Universität Frankfurt, August-Euler-Str. 6, D-60486 Frankfurt, Germany
[2] Research School of Physical Sciences and Engineering, Australian National University Canberra ACT 0200, Australia
[3]Centre for Atomic, Molecular and Surface Physics, Murdoch University, Perth, 6150 Australia
[4] Dept. of Physics, Western Michigan Univ., Kalamazoo, MI 49008
[5] Dept. of Physics, Kansas State Univ., Cardwell Hall, Manhattan KS 66506
[6] Lawrence Berkeley National Lab., Berkeley CA 94720

How does a single photon couple to two electrons in an atom? This question has been extensively discussed in the literature. Most of this discussion has been focused on the photo double ionization (PDI) of the helium atom which is the simplest two-electron-single-photon process. It is generally believed that at high photon energies the shake-off mechanism makes the largest contribution to PDI. The shake-off is a relaxation of the correlated initial state onto the new $He^+$ eigenstates after a sudden removal of one atomic electron. In contrast, close to the threshold, mainly one electron absorbs the photon and knocks out the second electron in an (e,2e) like collision (the process which is called in the literature the two-step-one, or TS1). The whole discussion on the PDI mechanisms is based solely on theory and on measured total cross sections. Differential data were available only in the regime of low energies, where the long range interaction between the electrons completely masks the signatures of the ionization mechanisms.

In this joint experimental and theoretical work we provide the first direct evidence for both mechanism by measuring the angular distributions of the photoelectrons by use of the COLTRIMS technique (Cold Target Recoil Ion Momentum Spectroscopy). The experiments have been performed at Bl. 4. They cover double ionization by linear and circular polarized light.

The following observations present the arguments for a two-step picture in which one electron absorbs the photon energy and its angular momentum and, subsequently, the second electron is either shaken-off or knocked out. The top panel of 1 shows the measured and calculated SDCS. It has a characteristic U-shape and peaks sharply at 0 eV

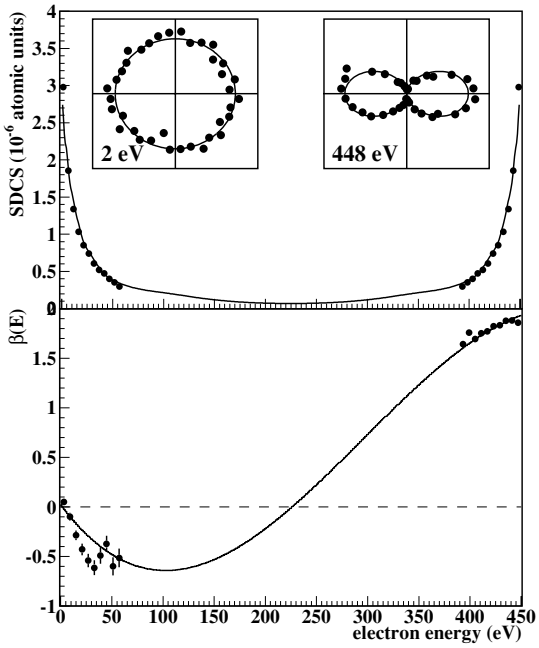


Figure 1: PDI of He at $\hbar\omega = 529$ eV. a) SDCS $d\sigma/dE$. The line is a CCC calculation. The insets show the DDCS $d\sigma^2/(d\Omega dE)$ at $E = 2$ eV and 448 eV. b) The asymmetry parameter $\beta$ versus the electron energy.

and 450 eV. This run of the curve is in contrast to the SDCS close to the threshold which is almost flat. The bottom panel of 1 shows the measured and calculated $\beta$ parameter. We find an angular asymmetry parameter $\beta \simeq 2$ for the very fast electrons and $\beta \simeq 0$ for the very slow electrons. Two examples of the experimental DDCS at $E = 2$ eV and 448 eV are shown in the insets together with the line obtained from CCC estimates of the SDCS and $\beta$. A very asymmetric energy sharing together with an angular asymmetry parameter $\beta \simeq 2$ for the fast electron indicate that the fast electron absorbs not only most of the photon energy but also its angular momentum. This directly suggests an interpretation of the PDI as a two-step process with the fast electron being the primary photoelectron. The very slow electrons are emitted isotropically at very low energies as expected for the shake-off, while $\beta$ becomes slightly negative for higher energies indicating a major role of the TS1 at higher energies of the slower electron.

After establishing the validity of a two step picture we show now, that the second step of the PDI is dominated by the shake-off mechanism for very low energetic electrons (about 1 eV), while 30 eV electrons are created mainly by a binary (e,2e) like collision. In brief, the shake-off results in a almost isotropic, slightly backward directed emission of the slow electron with respect to the fast one, while any binary collision between the electrons leads to an angle of 90 deg between them.

The TDCS for electrons $E_2 < 3$ eV (figure 2b) has a pear-like shape peaked at 180° to the fast electron. Contrary to all TDCS reported at lower photon energies so far, these slow electrons show a significant intensity for parallel emission into the same direction. This is possible because of the very asymmetric energy sharing of the two electrons. The

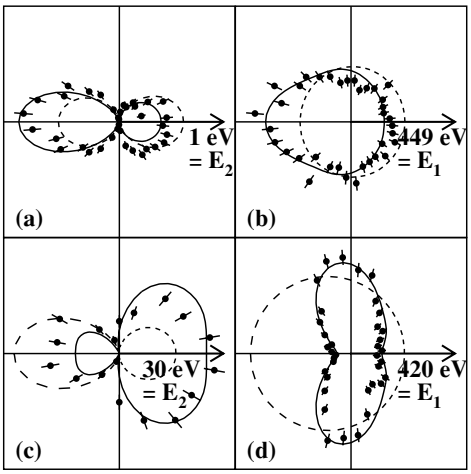


Figure 2: TDCS of the He PDI at 529 eV photon energy. In all panels the electrons are coplanar within $\pm 25°$, the polarization axis is horizontal. The direction and the energy of one of the two electrons is fixed as indicated by the number and the arrow, i.e. the slow electron is fixed in panels (a) and (c) and the fast electron is fixed in (b) and (d). The polar plots show the angular distribution of the complementary electron. The upper panels (a) and (b) are for the case $E_2 \simeq$ 2 eV; the lower panels have $E_2 \simeq$ 30 eV. The solid line is a full CCC calculation, the dashed line is a shake-off only CCC calculation. The measurements are normalized to the full CCC calculation.

solid line is a full CCC calculation which is in excellent agreement with the measurements.

The TDCS for electrons $E_2 \simeq 30$ eV (figure 2 c,d) are completely different from the low energy ones. We find emission of the electron into a narrow cone at 90° to the fast electron (figure 2 d). An angle of 90° between the electrons is expected from a binary collision between the electrons.

## ACKNOWLEDGMENTS

Many thanks to E. Arenholz and T. Young and the staff of the ALS extraordinary support during our beam time. R. D. acknowledges many enlightening discussions with J. Berakdar, A. Becker and S. Keller.

This work was supported in part by BMBF, DFG, the Division of Chemical Sciences, Geosciences and Biosciences Division, Office of Basic Energy Sciences, Office of Science, U. S. Department of Energy and the Director, Office of Science, Office of Basic Energy Sciences. The computations were performed at the National Facility of the Australian Partnership for Advanced Computing. R. D. was supported by the Heisenberg Programm der DFG. A. K. and Th. W. thank Graduiertenförderung des Landes Hessen for financial support.

Principal investigator: Reinhard Dörner, Institut fuer Kernpyhsik, August Euler Str. 6, D-60486 Frankfurt, Germany, email: doerner@hsb.uni-frankfurt.de, phone: 049 69 798 24218

# Multi-Atom Resonant Photoemission Effects from Solid Surfaces and Free Molecules

N. Mannella[1,2], B.S. Mun[1,2], S.-H. Yang[2], A.W. Kay[1,2,#],F.J. Garcia de Abajo[1,3], E. Arenholz[4], A.T. Young[4], Z. Hussain[4], H. Wang[5], O. Hemmers[5], D.W. Lindle[5], M.A. Van Hove[1,2], and C.S. Fadley[1,2]

[1]Dept. of Physics, University of California-Davis, Davis, CA 95616
[2]Materials Sciences Division, Lawrence Berkeley National Laboratory, Berkeley, CA 94720
[3] Centro Mixto CSIC-UPV/EHU, San Sebastian, Spain
[4]Advanced Light Source, Lawrence Berkeley National Laboratory, Berkeley, CA 94720
[5]Dept. of Chemistry, University of Nevada, Las Vegas, NV 89154
[#]Present address: Intel Corporation, Portland, OR

## INTRODUCTION

In prior work at the ALS, it has been pointed out that a new type of interatomic resonant photoemission effect exists, and that this effect furthermore has the potential of providing a useful probe of near-neighbor atomic identities, bonding, and magnetism [1-5]. The phenomenon has been termed multi-atom resonant photoemission (MARPE). In measuring this effect, the photoelectron intensity of a given core level from atom "A" (e.g. O 1s from MnO) is monitored while the photon energy is tuned through a strong absorption edge for a core level on another atom "B" in the sample (e.g. the Mn 2p edges in MnO). Initial observations on MnO and other metal oxides appeared to show significant entirely-positive interatomic resonant effects in photoemission of up to 100% [1]. Additional measurements in Auger emission and soft x-ray emission from MnO seemed to confirm that such effects were also present in secondary decay processes as a result of resonant enhancement of the initial O 1s core hole formation [2]. A theoretical model for these effects based on the extension of intraatomic resonant photoemission ideas to the interatomic case was also developed and compared favorably with experiment [3]. Other measurements on transition-metal compounds [6] and an adsorbate-substrate system [7a] seemed to confirm these measurements and analysis.

Subsequently, it has been realized that such experimental measurements require very careful allowance for potential detector non-linearities [4,5,7b], since the observed electron intensities (particularly inelastically scattered backgrounds) change dramatically in going over any core resonance. In particular, the detector used for several of the first MARPE studies [1,2,4-7a], the standard microchannel plate-plus-phosphor-plus-CCD camera incorporated in the Gammadata-Scienta series of electron spectrometers, exhibits not only a typical saturation effect for high countrates, but also a strong quadratic component of counting that goes above linear for low countrates. Thus, spectra obtained in this low-countrate regime, while not exhibiting any kind of saturation effect, can be artificially enhanced in intensity in passing over a core-level resonance. Methods of accurately correcting spectra for these non-linearities have been discussed [4,5,7b, and abstract by Mannella et al. in this 2001 Compendium]. When these effects are allowed for, the magnitude of the effect is reduced and the form is found to change, with the shape usually involving a negative-then-positive swing in intensity reminscent of a Fano profile in form [4,5,7b,8].

We here report more recent experimental results providing further evidence of such interatomic resonant effects in photoemission, for two very different limiting-case types of systems: a cleaved single-crystal oxide-NiO and a free molecule-$SF_6$. These data are discussed in terms of existing theoretical models for such MARPE effects [3,5], in particular, an x-ray optical (dielectric) approach that well describes the NiO data and a microscopic quantum mechanical model that should be useful in describing the $SF_6$ data.

## EXPERIMENTAL PROCEDURE

The NiO measurements were performed on beamline 4.0.2 and made use of the Advanced Photoelectron Spectrometer/Diffractometer located there. Detector non-linearities were corrected for in all data presented here, using methods described elsewhere [4,5, and abstract in the 2001 Compendium]. A NiO single crystal was cleaved just before insertion into ultrahigh vacuum via a loadlock, then ion bombardment and annealing in oxygen to remove minor surface contaminant levels and assure correct stoichiometry before measurement. The incidence angle of the radiation was varied from grazing values of 5° to much higher values up to 40° (cf. experimental geometry in Figure 1(a)).

The $SF_6$ measurements were performed on beamline 8.0.1 and made use of a time-of-flight spectrometer described in detail elsewhere [9]. The detectors in this spectrometer are positioned in angle with respect to the incoming radiation and polarization vector such that non-dipole contributions to the angular distributions can be readily measured with high accuracy. For reference, the angular distributions of photoelectrons from a randomly oriented ensemble of free molecules is given by $d\sigma / d\Omega = (\sigma / 4\pi)\{ 1 + \beta P_2(\cos\Theta_e) + [\delta + \gamma \cos^2\Theta_e] \sin\Theta_e \cos\Phi_e \}$, with $\beta$ the dipole asymmetry parameter and $\delta$ and $\gamma$ the first-order non-dipole parameters (cf. geometry in Figure 2(a), with $\Phi_e$ being the azimuthal angle around the polarization vector $\boldsymbol{\varepsilon}$) [9].

## EXPERIMENTAL RESULTS AND DISCUSSION

**NiO(001):** In Figure 1, we show experimental O 1s intensities from NiO as a function of photon energy and for five different x-ray incidence angles. For the lowest incidence angle of 5°, the effect of crossing the Ni 2p absorption resonances is dramatic, yielding a negative-then-positive excursion on crossing $2p_{3/2}$ whose amplitude is 75% of the intensity below the resonance. The magnitudes of these effects decreases as the incidence angle is increased, falling off to about 5% for an incidence angle of 40°.

Also shown in Figure 1 are theoretical curves based on an x-ray optical model of such effects, as discussed previously [5]. The optical constants that are key inputs for this model have been derived from concomitant partial-yield x-ray absorption measurements, with corrections for x-ray incidence angle and secondary electron takeoff angle [4], and subsequent Kramers-Kronig analysis [5]. The resulting theoretical curves are in excellent agreement with experiment for the lowest angle, and the agreement is very good for all other angles as well, although with some overprediction of the amplitudes at the higher angles. Non-zero effects are observed and predicted over the full angle range, in qualitative agreement with prior data for MnO [5]. These data thus disagree with one aspect of an earlier study of NiO by Finazzi et al. [8], in which they did not observe any sort of MARPE effect in O 1s emission from NiO; this lack of any effect appears to be due to measuring with too high an incidence angle and having insufficient statistical accuracy to resolve the small remaining effects seen, e.g. in Figures 2(e)-2(f).

We thus expect such MARPE effects to be observable in photoemission from any solid surface, with strength depending on the relative intensities of the absorption resonances. Furthermore, for homogeneous systems with flat surfaces, the x-ray optical model should provide a reasonably quantitative picture of the observed phenomena. Effects following an x-ray optical analysis have also recently been observed for photoemission from an adsorbate on a metal-$N_2$/Ni(001) [10]. For more complex cases with, e.g., three-dimensional nanometer-scale heterogeneity, the use of a microscopic model will be more appropriate.

**$SF_6$:** In Figure 2, experimental results for $SF_6$ are summarized. The x-ray absorption coefficient is shown in Figure 2(b), and the S 2p photoemission intensity and its asymmetry parameters were measured as photon energy was scanned across the "A" absorption resonance (corresponding to a F

$1s\ t_{1u}$-to-$a^*_{1g}$ excitation). Although the total S 2p intensity (proportional to $\sigma$) does not show a significant change in crossing the resonance (≤few %), the dipole asymmetry parameter $\beta$ (as shown in Figure 2(b)) exhibits about a 15% excursion in magnitude that is also of the same general form as those in Figure 1. Similar effects are also seen in the parameters $\delta$ and $\gamma$ [11].

Thus, interatomic resonant effects are also seen in this free molecule, and although they are too small to be observed as yet in the total intensity, they are clearly observed in the various asymmetry parameters. No theoretical calculations have as yet been performed for this case, but the x-ray optical model would clearly be inappropriate, and a microscopic approach such as that discussed previously [3,5] is the logical starting point for understanding these effects.

## CONCLUSIONS

Multi-atom resonant photoemission effects are found in both the total intensities from homogeneous solid surfaces and adsorbates on such surfaces, for which an x-ray optical model is found to well describe the data, and in the angular distribution asymmetry parameters of a free molecule, for which a microscopic theoretical approach will be necessary. Similar effects in nanoscale structures will lie somewhere between these two cases.

## REFERENCES


1. A. Kay, E. Arenholz, B.S. Mun, F.J. Garcia de Abajo, C.S. Fadley, R. Denecke, Z. Hussain, and M.A. Van Hove, *Science* **281**, 679(1998).
2. (a) E. Arenholz, A.W. Kay, C.S. Fadley, M.M. Grush, T.A. Callcott, D.L. Ederer, C. Heske, and Z. Hussain, *Phys. Rev. B* **61**, 7183 (2000); (b) E. Arenholz, A.W. Kay, unpublished results.
3. F.J. Garcia de Abajo, C.S. Fadley, and M.A. Van Hove, *Phys. Rev. Lett*. **82**, 4126 (1999).
4. A.W. Kay, Ph.D. dissertation (University of California-Davis, September, 2000), Chapters 4 and 5.
5. A.W. Kay, F.J. Garcia de Abajo, S.H. Yang, E. Arenholz, B.S. Mun, M.A. Van Hove, Z. Hussain, and C.S. Fadley, Physical Review B **63**, 5119 (2001).
6. A. Kikas, E. Nommiste, R. Ruus, A. Saar, and I. Martinson, Sol. St. Commun. **115**, 275 (2000).
7. (a) M.G. Garnier, N. Witkowski, R. Denecke, D. Nordlund, A. Nilsson, M. Nagasono, and N. Mårtensson, and A. Föhlisch, Maxlab Annual Report for 1999 and private communication correcting this data; (b) D. Nordlund, M. G. Garnier, N. Witowsky, R. Denecke, A. Nilsson, M. Nagasono, N. Mårtensson and A. Föhlisch, Phys. Rev. B **63**, 121402 (2001).
8. M. Finazzi, G. Ghiringhelli, O. Tjernberg, L. Duo, A. Tagliaferri, P. Ohresser, and N. B. Brookes, Phys. Rev. B **62**, R16215 (2000).
9. (a) O. Hemmers et al., Rev. Sci. Instrum. **69**, 3809 (1998); (b) O. Hemmers et al., Phys. Rev. Lett. **87**, 273003 (2001).
10. D. Menzel, W. Wurth, A. Föhlisch, P. Fuelner, S.-H. Yang, and C.S. Fadley, private communication.
11. H. Wang, O. Hemmers, P. Focke, M. M. Sant'Anna, D. Lukic, C. Heske, R. C. C. Perera, I. Sellin, and D. Lindle, to be published.



This work was supported by the U.S. Department of Energy, Office of Science, Office of Basic Energy Sciences, Materials Sciences Division, under Contract No. DE-AC03-76SF00098, and the National Science Foundation.



Principal investigator: N. Mannella, Department of Physics UC Davis, and Materials Sciences Division, Lawrence Berkeley National Laboratory. Email: norman@electron.lbl.gov. Telephone: 510-486-4581


Figure 1. (a) Experimental geometry for measurements on Ni(001). (b)-(f) O 1s intensity as photon energy is scanned through the Ni $2p_{1/2\text{-}3/2}$ absorption resonances. Both experimental data (blue points) and theoretical calculations based on an x-ray optical model (red curves) are shown.

Figure 2. (a) Experimental geometry for measurements on gas-phase $SF_6$. (b) The x-ray absorption coefficient in the F 1s region as measured by partial electron yield. (c) The dipole asymmetry parameter β as photon energy is scanned through the "A" resonance in (b).

**Figure 1.**

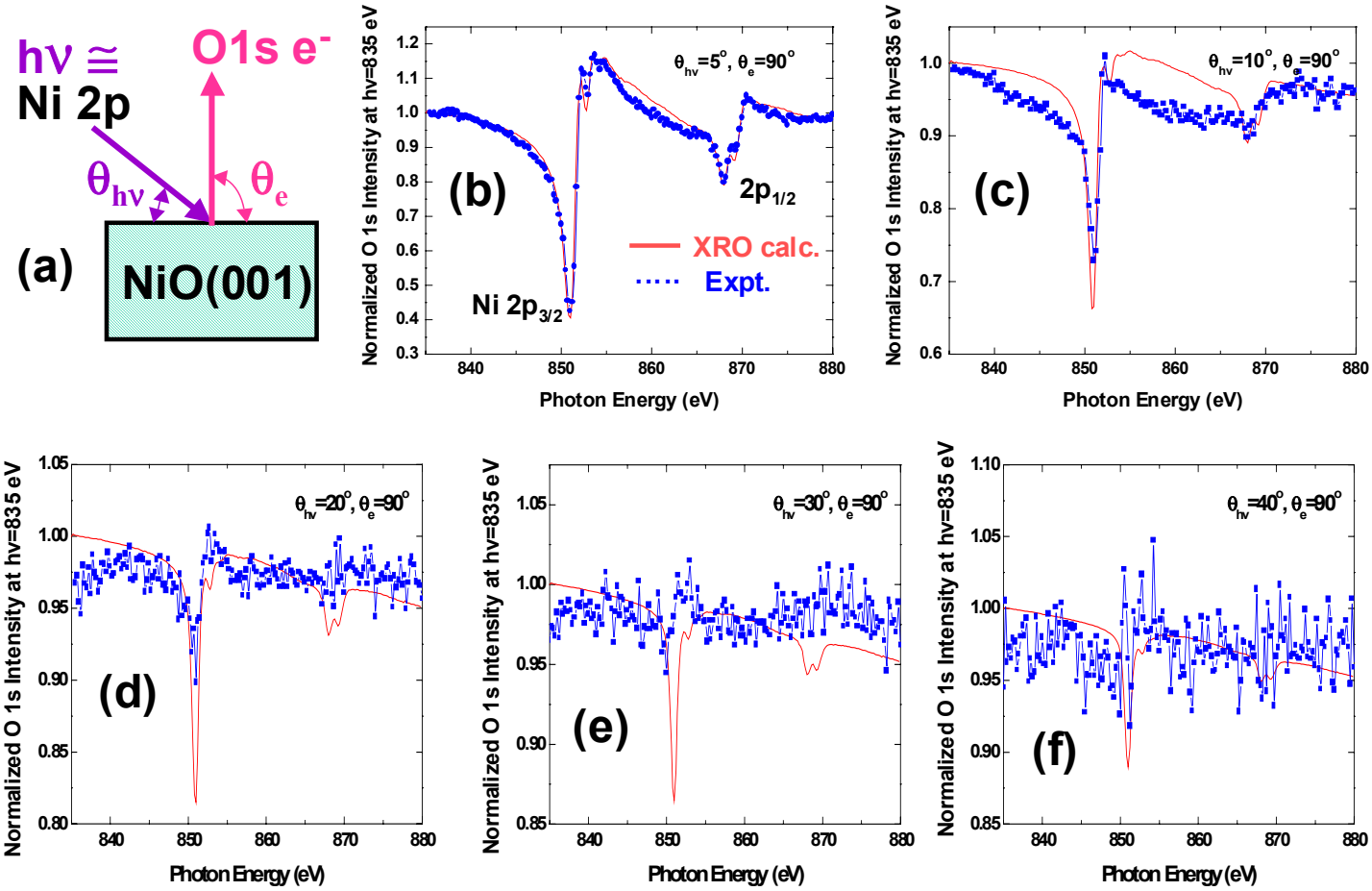


**Figure 2.**

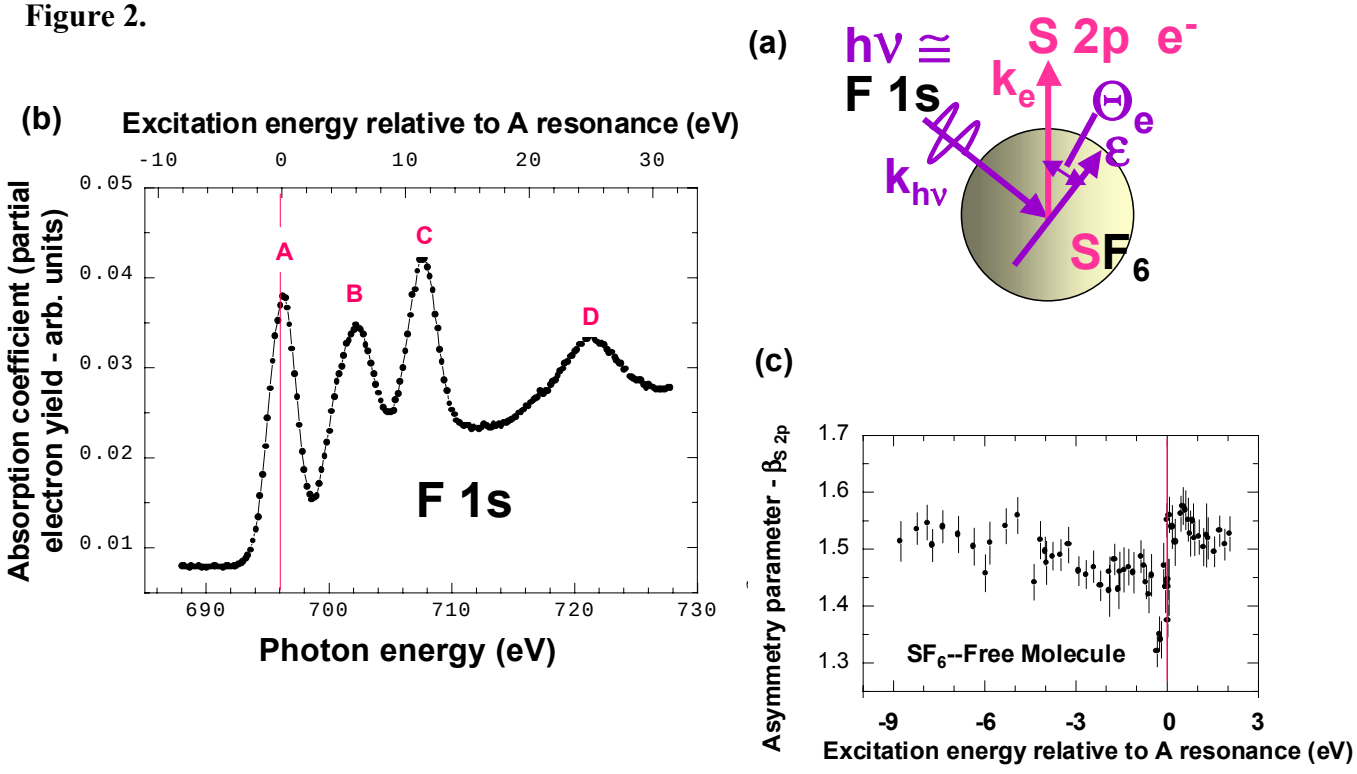

# Resolving magnetic and chemical correlation lengths in CoPtCr-based recording media

O. Hellwig,[1] J. B. Kortright,[2] D. T. Margulies,[1] B. Lengsfield,[1] and E. E. Fullerton[1]
[1]IBM Almaden Research Center, San Jose, California 95120, USA
[2]Materials Sciences Division, Ernest Orlando Lawrence Berkeley National Laboratory, University of California, Berkeley, California 94720, USA

## GRANULAR RECORDING MEDIA

Current magnetic recording media consists of chemically segregated, polycrystalline grains whose grain-centers are ferromagnetic with in-plane anisotropy and whose grain boundaries are nominally non-magnetic [1]. This chemically and magnetically heterogeneous microstructure has evolved through several generations of recording media via an increasingly complex set of alloys from CoCr to CoPtCr to CoPtCrB. The additives Cr and later B are known to segregate to and produce nonmagnetic grain boundary phases that were believed to reduce exchange coupling between adjacent grains, thereby enabling sharper bit transitions and higher recording density [2]. Chemical heterogeneity associated with these films is resolved using high-resolution TEM and micro-EELS [3]. It has remained difficult, however, to directly measure the magnetic correlation lengths giving the distance over which grain-to-grain magnetism is correlated.

We have found that both magnetic and chemical heterogeneity in recording media films are strong scattering sources when tuned to specific soft x-ray core resonances to enhance contrast [4,5]. This transmission small-angle scattering (SAS) measurement positions the scattering vector $q$ in the film plane to optimize coupling to in-plane structure (Fig. 1b, inset) [6]. Although soft x-ray wavelengths limit the maximum $q$, spatial resolution to 1 nm is available.

## Q-RESOLVED RESONANT SCATTERING

SAS $q$ scans measured at the resonant intensity peaks at the Co and Cr $L_3$ lines are shown in Fig. 1. Scans of the common underlayer structure (without any media layer) reveal the contributions from the underlayer and the SiN membrane. These scans are almost featureless, with enhanced low $q$ scattering that is also observed in scattering from the substrate alone, and with a weak, broad peak at $q \cong 0.015$ Å$^{-1}$ observed at the Cr resonance. For the samples with media layers there is additional, strong SAS at both the Cr and Co edges arising from the media layer. This scattering is strongly resonantly enhanced, as is illustrated in Fig. 1b by the 10-fold decrease in scattering just 10 eV below the Co $L_3$ peak (dashed line) compared to that measured at the peak (open circles). Similarly strong and sharp resonant enhancements are observed near the Cr $L_3$ line.

The SAS scans from the different media samples show similar features. The Cr-edge data has a peak at $q \cong 0.07$ Å$^{-1}$ for all samples. This peak results from interference between neighboring scattering centers separated by $2\pi/q \cong 100$ Å, typical of grain diameters observed in TEM images of media grown on similar underlayers [2]. We attribute this Cr resonant peak to the average grain diameter of the media. It is well established that chemical segregation during the growth of CoCr alloys involves Cr diffusion to the grain boundaries resulting in a magnetic Co-rich core of the grain with non-magnetic or weakly magnetic Cr-rich grain boundaries [6,7], as shown schematically in Fig. 1b. Thus, by tuning to the Cr edge, we enhance the chemical contrast between the magnetic grain core and the Cr-rich grain boundaries.

The Co-edge scattering is expected to arise from both magnetic and chemical correlations (and their interference). These data show the same interference peak at $q \cong 0.07$Å$^{-1}$ that was observed in the

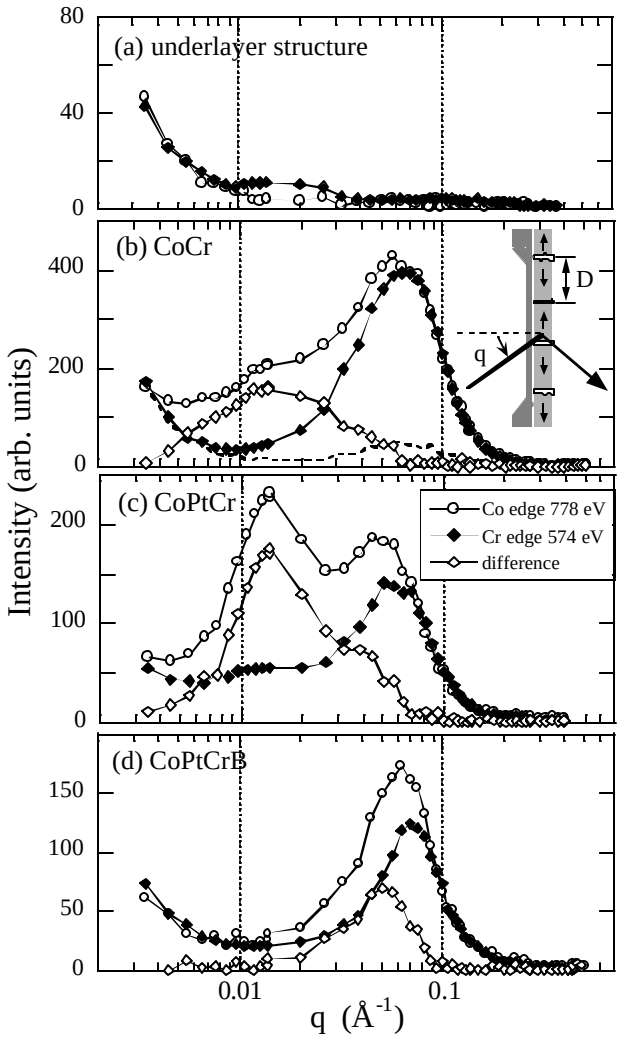


Figure 1. Resonant SAS from the underlayer structure without media layer (a) and from CoCr (b), CoPtCr(c), and CoPtCrB (d) media measured at the Co and Cr L3 lines as indicated. The inset shows the scattering geometry and media layer with magnetic grains (diameter D) with the in-plane magnetization direction represented by the arrows and nonmagnetic grain boundaries. The open diamonds are the difference between the Co- and Cr-edge data. The dashed line in (b) is the nonresonant scattering measured 10 eV below the Co edge.

Cr-edge data, as well as additional scattering at significantly lower $q$ values. The observation of high-$q$ resonant scattering from the grain structure at both the Co and Cr edges confirms that this scattering arises from in-plane compositional variations of Co and Cr. The additional lower-$q$ scattering arises predominantly from correlated magnetic regions larger than the grain size. For the CoPtCr film (Fig. 1c), this additional scattering is clearly resolved as a peak at $q \cong 0.015$ Å$^{-1}$ corresponding to a real space distance of ≅ 400 Å. The difference of the Co and Cr resonant scans (scaled to match at high $q$) results from Co magnetic-magnetic correlations and magnetic-charge interference, with the former dominating the low-$q$ peak and the latter contributing progressively to increasing $q$. The low-$q$ peak is thus a measure of the magnetic correlation length in these media films.

Boron additions are seen to reduce the magnetic correlation length from 4-5 times the chemical grain size to closely approach the grain size, consistent with improved recording performance and inferred magnetic correlation lengths from recording signal to noise measurements.

**MODELING ENERGY SPECTRA**

The above interpretation of magnetic and chemical peaks is qualitative. One approach to independent, quantitative determination of the scattering sources contributing to the peaks is to model the energy spectra of the scattering at each peak [5]. Measured Co $L_3$ energy spectra at these two peaks for the CoPtCr sample are shown as symbols in Fig. 2, and clearly have very different shape. Modeling these resonant shapes requires measured values of charge and magnetic atomic scattering factors $f$ for Co. These were obtained from transmission absorption measurements of the saturated media film with linear and circular polarization, followed by Kramers-Kronig transformation of the imaginary part of these quantities to obtain their real parts. Non-resonant $f$ values for Cr and Pt were taken from tabulated values [9].

Following standard SAS formalisms, the amplitude for different scattering sources is given by the difference of amplitudes of the two phases defining the heterogeneity. The simplest model for pure magnetic scattering yields amplitude proportional to the magnetic part of $f$ for Co [5, 6]. The corresponding intensity is scaled and plotted in Fig. 2, with a small non-resonant background added.

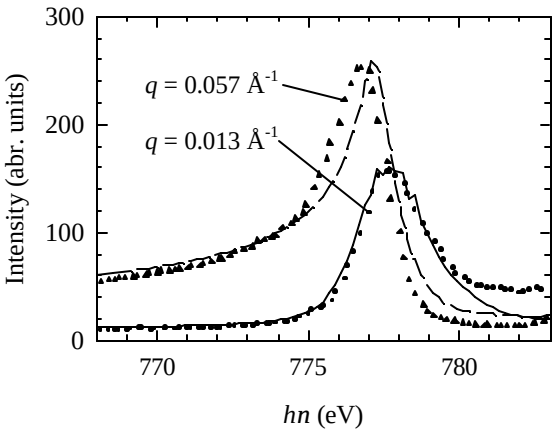


Figure 2. SAS energy spectra across the Co $L_3$ line of the CoPtCr media at the high- and low-$q$ peaks (symbols). Model spectra based on measured Co resonant scattering factors (lines) confirm the magnetic and chemical origin of the two peaks.

The good agreement of model and measured spectra confirms the magnetic origin of the low-$q$ peak and thus that magnetic correlation lengths in this sample are several times the chemical grain size. Modeling the high-$q$ spectrum requires postulating compositions of the segregated phases at the grain boundaries and centers, forming the appropriate scattering amplitudes of these two phases as linear combinations of elemental scattering factors, and squaring the difference of these amplitudes to obtain the intensity spectrum. A model spectrum is scaled and plotted with the high-$q$ data in Fig. 2, confirming that the high-$q$ peak is consistently modeled assuming chemical origin. Details showing that this model is sensitive to the composition of segregated phases are in ref. [5].

## CONCLUSIONS

Resonant SAS contrast at Co and Cr $L_{2,3}$ lines strongly enhances both magnetic and chemical scattering in recording media films. Since Co and Cr enhancements have different sensitivity to chemical and magnetic heterogeneity, their relative behavior allows clear separation of chemical and magnetic length scales and a very direct measurement of magnetic correlation lengths in granular recording media. The addition of B to the media alloys significantly reduces the magnetic correlation lengths [4]. Modeling of resonant energy spectra at the Co $L_3$ edge using measured resonant Co scattering factors quantitatively confirms magnetic and chemical scattering sources and provides an estimate of the composition of segregated phases yielding the chemical scattering [5].

## REFERENCES

1. H. N. Bertram, Theory of Magnetic Recording (Cambridge University Press, Cambridge, U.K.) 1994.
2. M. Doerner, *et al*., IEEE Trans. Magn. 37 (2001) 1052.
3. M. Doerner, *et al*., IEEE Trans. Magn. 36 (2000) 43.
4. O. Hellwig, D. T. Marguiles, B. Lengsfield, E. E. Fullerton, J. B. Kortright, Appl. Phys. Lett. 80 (2002) 1234.
5. J. B. Kortright, O. Hellwig, D. T. Marguiles, E. E. Fullerton, J. Magn. and Magn. Mater. 240 (2002) 325.
6. J. B. Kortright, *et al.*, Phys. Rev. B 64 (2001) 092401.
7. J. E. Wittig, *et al*., IEEE Trans. Magn. 34 (1998) 1564.
8. N. Inaba, Y. Uesaka, and M. Futamoto, IEEE Trans. Magn. 36 (2000) 54.
9. B. L. Henke, E. M. Gullikson, J. C. Davis, At. Data Nucl. Data Tables 54 (1993) 181; and at http:/www-cxro.lbl.gov/optical_constants/.

This work and JBK were supported by the Director, Office of Energy Research, Office of Basic Energy Sciences, Materials Science Division, of the U.S. Department of Energy under Contract No. DE-AC03-76SF00098.

Principal investigator: Eric Fullerton, IBM Almaden Research Center. Email: eef@almaden.ibm.com. Telephone: (408) 927-2430.

# Spin-Resolved Electron Spectroscopy of Carbonyl Sulphide

G. Turri[1,2], G. Snell[1], B. Langer[3], M. Martins[4], E. Kukk[5], P. Langhoff[6,7,8] and N. Berrah[1]

[1]Western Michigan University, Department of Physics, Kalamazoo, MI 49008, USA
[2] Lawrence Berkeley National Laboratory, Advanced Light Source division, Berkeley, CA 94720, USA
[3] Fritz-Haber-Institut der Max-Planck-Gesellschaft, 14195 Berlin, Germany
[4] Freie Universität Berlin, Institut für Experimentalphysik, 14195 Berlin, Germany
[5] Dept. of Physics, Oulu University, 90570 Oulu, Finland
[6] Air Force Research Laboratory, AFRL/PRS, Edwards AFB, California 93524-7680
[7] Department of Chemistry, Indiana University, Bloomington, Indiana 47405
[8] San Diego Supercomputer Center, University of California, 9500 Gilman Drive, La Jolla, California 92093-0505

## Introduction

Energy- and angle-resolved photoelectron spectroscopy has been widley used to investigate the structures of atoms, molecules and solid matter as well as the dynamics of photoemission processes. Though, the information that can be obtained with this technique is often incomplete, even when the most simple systems are investigated [1]. Quantum mechanically the photoemission process is described in terms of the wavefunctions for the initial and final states and the Coulomb or dipole transition matrix elements. The determination of all the matrix elements of one physical process is the aim of the so-called complete (or perfect) experiment [2,3]. This definition is clearly model dependent [3].

Different techniques have been introduced to tempt a complete photoionization experiment. Some make use of coincidence between electron and electron [4,5,6] , or electron and fluorescent photon [7,8]. Other take advantage of the properties of polarized atoms [9,10]. The possibility of using spin-resolved electron spectroscopy has been theoretically described by Huang for photoionization [11] and Auger decay [12]. Since then, this technique has been widley used in experiments, see [13,14,15] for example.

Despite the substantial advancements of complete experiment in atomic systems, there have been only very few studies of inner-shell photoionization of molecules beyond intensities and angular distributions [16]. A molecular complete experiment is much more difficult than the determination of matrix elements for atoms, because of the large number of possible outgoing partial waves. Additionally, the molecular environment can influence the core orbitals of the atoms in the molecule. This can lead to the splitting of energy levels due to vibrations, lower than spherical symmetry of the system, etc.

In this work we report on spin polarization measurements of the sulphur 2p photoionization of carbonyl sulphide molecule. Recently, Kukk et al. [17] investigated the sulphur 2p photoionization of OCS molecules by high-resolution, angle-resolved electron spectroscopy. They found that the angular distribution parameter $\beta$ of the two molecular-field-split components of the sulphur $2p_{3/2}$ line differs significantly at a broad range of photon energies above the 2p threshold. Since the origin of this difference cannot be traced solely by angle-resolved spectroscopy, we measured the spin polarization of the S 2p lines. The analysis of the acquired data is still in progress; some preliminary results will be presented here.

## Experiment

The experiment was performed at Beamline 4 at Advanced Light Source (ALS) storage ring. We used circularly and linearly polarized light from the new elliptical polarization undulator (EPU) [18]. The sulphur 2p photoionization was measured for 6 different photon energies, namely 185, 191, 195, 205, 220 and 260 eV. With the chosen setting of the parameters of the beamline, a photon flux of approximately $10^{14}$ photons/sec and a resolving power $E/\Delta E$

about 1000 was provided. The degree of both circular and linear polarization for all the photon energies was 100% within the experimental errors. The photon beam crossed perpendicularly an OCS effusive gas jet. The kinetic energy of the photoemitted electrons was measured with two Time Of Flight (TOF) spectrometers. Combined with one of the TOF, a spherical Mott polarimeter of the Rice type, operated at 45KV, performed the spin polarization analysis. The instrumental asymmetry of the Mott polarimeter was accounted by combining measurements with positive and negative light helicity [19], changing polarization approximately every 10 min. Due to the substantial loss of signal intensity during the Mott scattering, our experiment considerably benefited from the TOF technique's inherent capability of simultaneous acquisition of all lines in the spectrum.

**Results**

The sulphur 2p-photoionization spectrum of OCS, as measured with 205 eV circularly polarized photon, is reported in the lower panel of Fig.1 (sum of the spectra with different spin polarization).

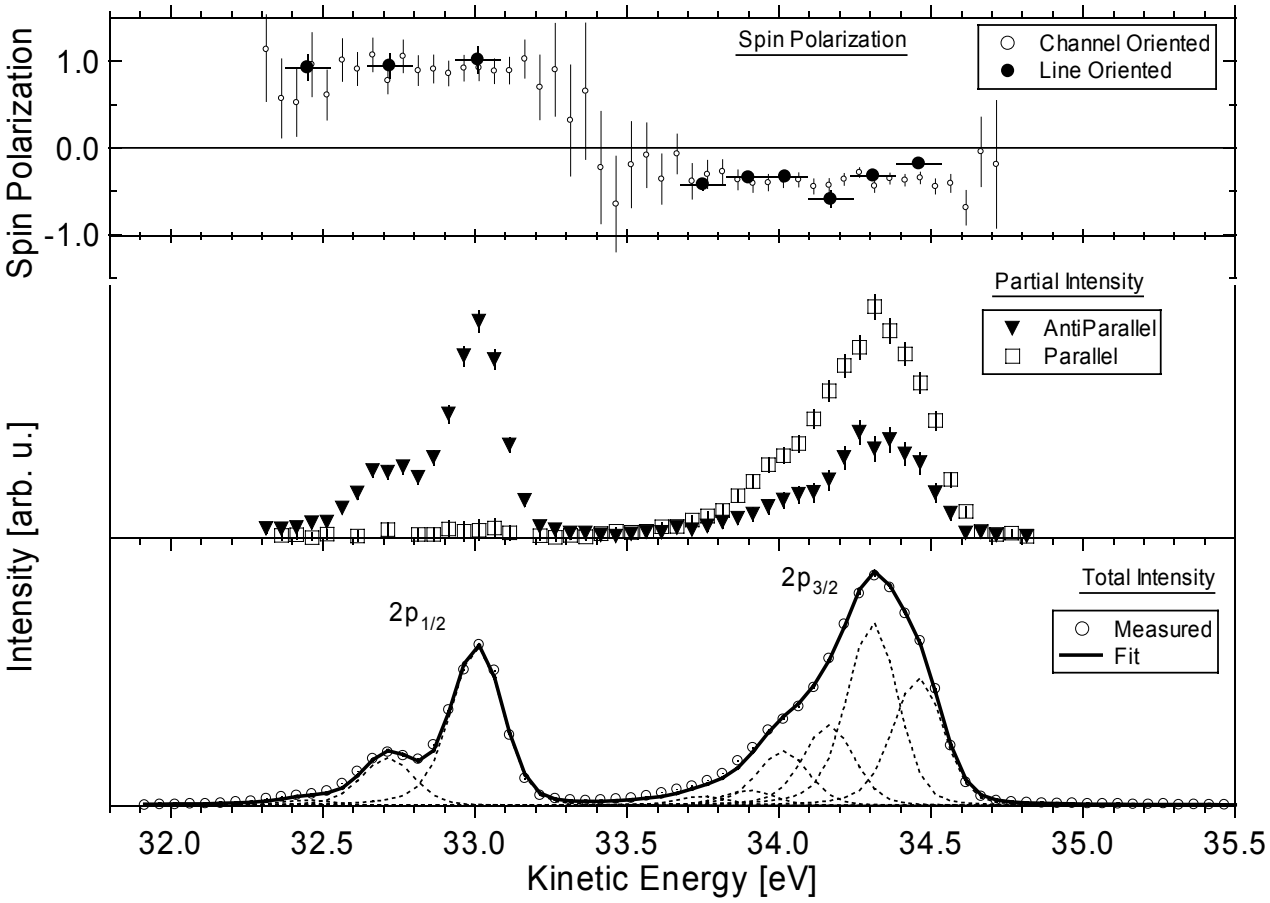


Fig.1: Sulphur 2p-photoionization spectrum of OCS molecule, as measured with 205 eV circularly-polarized photon. (bottom) Total Intensity, the continuous curves are the result of a least-squares fitting procedure. (middle) Spin-Separated Intensity. (up) Spin Polarization. See text for details.

As described in details by Kukk et al. [17] the spectrum can be completely understood in terms of spin-orbit, vibrational and molecular field split. Within the resolution of our experiment, the two spin-orbit components are easily resolved; in order to solve the vibrational and molecular field splitting, we applied a least-squares fitting procedure, using asymmetric Voight profiles.

We applied two different techniques to extract the spin polarization from our data. The areas of

the different peaks, as returned by the fitting procedure, were used to obtain the polarization of the different components of the spectrum. This technique has been referred as a "Line-Oriented" analysis [15]. Alternatively, we applied a "Channel-Oriented" analysis, where the spin polarization has been calculated for each point of the photoemission spectra. The results of the two methods are reported in the top panel of Fig.1, showing good agreement. Using the values obtained with the latter analysis, we deduced the spin separated spectra [14], which correspond to the spectra that a "perfect" Mott polarimeter (i.e. with no instrumental asymmetry, and Sherman function equal to1) would measure in case of completely circularly polarized light. These spectra are reported in the middle panel of Fig.1.

Both the spin-orbit components show strong spin-polarization. Conversely, the vibrational and the molecular splitting show minor effect on the spin polarization at this photon energy. The polarization of the three states of the $2p_{1/2}$ peak is $+0.95 \pm 0.15$, i.e. these states are almost completely spin-polarized. This is reflected in the vanishing of the $2p_{1/2}$ peak in the spin separated spectrum associated with electron spin parallel to the photon spin. The states associated with the $2p_{3/2}$ peak show slightly different polarization values out of the error bars. The different sign in the spin polarization of the two spin-orbit states qualitatively agree with the fact that the polarization of the 2p photoionization line should vanish when the spin-orbit structure is not resolved.

## Conclusion

Whereas the most of the analysis has to be done, the few preliminary results seem to be encouraging. The investigated transitions show strong spin polarization, which makes them very suited for spin resolved technique. The agreement of the results obtained by using different analysis techniques confirms the consistency of the investigation.

## Funding

Department of Energy, Office of Science, Basic Energy Sciences, Chemical Sciences Division

## References

[1] B. Schmidtke et al., J. Phys. B **33**
[2] U. Heinzmann et al., J. Phys. B **13**, 4353 (1980).
[3] J. Kessler et al., Comments At. Mol. Phys.**10**, 47 (1981).
[4] N.M. Kabachnik et al., J. Phys.B **32**, 1769 (1999).
[5] K. Ueda et al., Phys. Rev. Lett. **83**, 5463 (1999).
[6] G. Turri et al., J. Elect. Spect. **114**, 199 (2001).
[7] J. Jimenez et al., Phys. Rev. Lett. **57**, 2260 (1986).
[8] H.-J. Beyer et al., J. Phys. B **28**, L47 (1995.)
[9] O. Plotzke et al., Phys. Rev. Lett. **77**, 2642 (1996.)
[10] K. Godehusen et al., Phys. Rev. A **58**, R3371 (1998).
[11] K.-N. Huang, Phys. Rev. A **22**, 223 (1980).
[12] K.-N. Huang, Phys. Rev. A **26**, 2274 (1982).
[13] G. Snell et al., Phys. Rev. Lett. **82**, 2480 (1999).
[14] U. Hergenhahn et al., Phys. Rev. Lett. **82**, 5020 (1999).
[15] G. Snell et al., Phys. Rev. A **63**, 032712 (2001).
[16] E. Shigemasa et al., Phys. Rev. Lett. **80**, 1622 (2000).
[17] E. Kukk et al., J. Phys. B **33**, L51 (2000)
[18] A.T. Young et al., Nuc. Instrum. and Methods A **467**, 549 (2001)
[19] T.J. Gay and F.B. Dunning, Rev. Sci. Instrum. **63**, 1635 (1992)

Principal investigator: Nora Berrah, Physics Department, Western Michigan University, Kalamazoo, MI 49008. Telephone: (1) 616-387-4955. Fax: (1) 616-387-4939. Email: berrah@wmich.edu.

# Variable Moments and Changing Magnetic Behavior of Thin-Film FeNi Alloys

M. Hochstrasser[1], J.G. Tobin[1], N.A.R. Gilman[2], R.F. Willis[2], S.A. Morton[3], and G.D. Waddill[3]
[1]Chemistry & Material Science Division, Lawrence Livermore National Laboratory,
Livermore, California 94550, USA
[2]Department of Physics, The Pennsylvania State University, University Park, Pennsylvania 16802, USA
[3]Department of Physics, University of Missouri-Rolla, Rolla, Missouri 65409, USA

## INTRODUCTION

The electronic properties and magnetic behavior of FeNi alloys have been of special interest since 1897 when Guillaume [1] first reported an almost zero thermal expansion over a wide temperature range in face-centered cubic (fcc) crystals with a Ni concentration of around 35 atomic percent. This behavior was subsequently observed in various ordered and random binary alloy systems, and became known as the "Invar Effect" [2]. Despite much experimental [3] and theoretical [4] work, a full understanding of this important technological effect is lacking.

A general view, first advanced by Weiss [3], is that the Fe atoms first develop a large magnetic moment in the Ni-rich alloys, which expands their lattice as their number increases. At a critical Wigner-Seitz cell volume, the strain energy becomes too large and there is a phase transition from this "high-spin/high-volume" state into a 'low-spin/low-volume" state. In the bulk alloys, this instability begins around 60% Fe content, the Curie temperature falling precipitously, simultaneously with a 'martensitic' structural transformation to body-centerd cubic (bcc) symmetry [2]. Theoretical work predicts that the fcc phase can exist in two possible states: a ferromagnetic high volume state or an antiferromagnetic low volume state (2 $\gamma$ state model) [3] with a volume change between the paramagnetic and the high spin state of ~7% [5], and 1% change between a non-collinear equilibrium state and the high spin state [4]. Experimental work shows a lattice expansion increasing linearly up to 3% at 65% Fe content followed by a sudden relaxation of 2% with increasing Fe content [6]. This work also shows that the martensitic structural transformation can be arrested in ultrathin alloy films epitaxially grown on a Cu(100) substrate. The nanometer-scale thickness effectively 'clamps' the crystal structure to that of the fcc substrate. Small changes in the Wigner-Seitz cell volume produce a small tetragonal distortion, which can be monitored by diffraction methods [6]. By growing ultrathin pseudomorphic fcc films, it is possible to focus on the effect of changing alloy composition on themagnetic and electronic behavior.

Here, we report changes in the magnitudes of both elemental magnetic moments with changing composition, measured with X-ray linear/circular dichroism as well as changes in the exchange splitting measured with spin- and angle-resolved photoemission.

## RESULTS AND DISCUSSION

A plot of the change in the asymmetry amplitude, for both elements in the FeNi alloy measured with XMLDAD, being a measure of the expectation value of the atomic magnetic moment $\langle\mu\rangle$, is shown plotted as a function of composition, fig. 1 (left panel). We observe that both the Ni and Fe signals track a similar profile with changing composition. In the Ni-rich alloys, both signal increase linearly up to 65% that on the Fe showing the larger increase. Above 65% Fe content, both signals show a sharp decrease. The observed asymmetry amplitudes, suggest that a high-spin moment develops on the Fe with increasing Fe content that increases overall magnetization,

which then increases the polarization of the valence states surrounding the Ni atomic cores. The Ni thus develops a component that tracks the developing magnetization. Above 65% Fe-content, the high-spin moment on the Fe appears to collapse to a "low-spin value", causing the overall magnetization density to be lowered, which is sensed by the reduced polarization of the valence states on the Ni. A plot of the variation of a 'stoichiometric average moment' $xA(Fe_x)+(1-x)A(Ni_{1-x})$ is shown in fig. 1 (right panel).. The behavior is very similar to that reported for the variation of the saturated moment normalized to the volume of similar fcc films on Cu(100) & Cu(111) and measured with SQUID magnetometry [7]. The solid line is the behavior reported for FeNi alloys from neutron scattering measurements [2]. We note that the Ni-rich phase extrapolates to a value around $\mu$=2.5-3.0$\mu$B, a value predicted theoretically for the "high-moment" metastable fcc phase [5]. The above 'mean magnetic moment' variation, normalizing the Ni asymmetry amplitude to be equivalent to the magnetic moment of metallic Ni is tracking closely the Slater-Pauling curve, the moment increasing linearly with increasing number of holes per atom in the valence electronic states. Above 65% Fe content, the average moment shows a sharp decline into a "low-spin" magnitude state, which could be the result of a collapse of the spin moment on the Fe atoms and/or a sudden decrease in magnetization due to a non collinear rearrangement of spins.

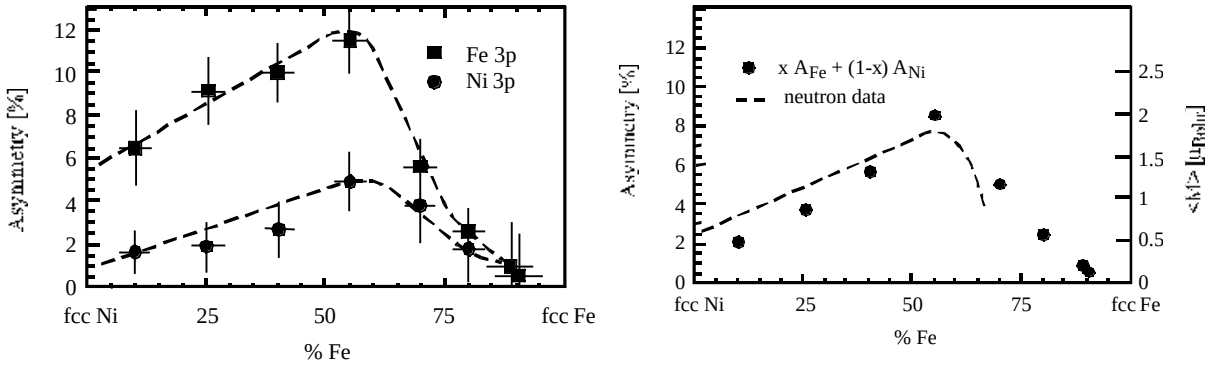


Figure 1. Left panel: Change in dichroism amplitude, A, as a function of FeNi alloy composition. Right panel: The variation of the 'stoichiometrically-weighted' dichroism signal amplitude (see text) with changing FeNi alloy composition. The dashed curve is the behavior observed in bulk FeNi alloys by neutron scattering. The right hand scale is determined from neutron and SQUID magnetometry data [2,7]

Spin polarized photoemission studies record a sudden decrease in the "mean-field" exchange splitting of the d-states with increasing Fe content through the critical "Invar transition". Angle-resolved photoemission imaging of states at the Fermi level [8] reveal a much smaller splitting of the sp-states, which also tracks the changing magnetization with changing composition. Spectral lineshapes reveal a decreased lifetime (i.e. decreased mean-free path for scattering) of the minority spin-polarized sp-states, in agreement with reported similar measurements on permalloy [9].Angle-resolved photoemission measurements of the sp-states, away from the regions of emerging minority d-states, along the <110> ($\Sigma$) symmetry direction, resolves the sp exchange splitting in reciprocal space. We observe that the spectral width of the minority-spin band of the sp-states is broader than that of the majority-spin sp-band.

This has been reported in similar measurements on permalloy, and is indicative of a shorter lifetime due to increased scattering and a shorter mean-free-path for the minority spin electrons. We also note that the lifetime broadening of the minority-spin sp-states increases significantly in the Fe rich alloys. The measured exchange splitting of the sp-states as well as the spin-resolved measured exchange splitting of the d-states track the behavior of the x-ray core-level photoemission dichroism.

This is to be expected on the basis of the overall magnetic energy being the sum of a 'local moment' energy on the 'atom(s) and a 'mean-field' exchange energy rising from the spin polarization of the itinerant valence states [10].
X-ray circular dichroism measurements allow to separate the orbital from the spin part of the local moments. Our measurements show the same concentration dependence of the local moments as t he linear dichroism measurements.

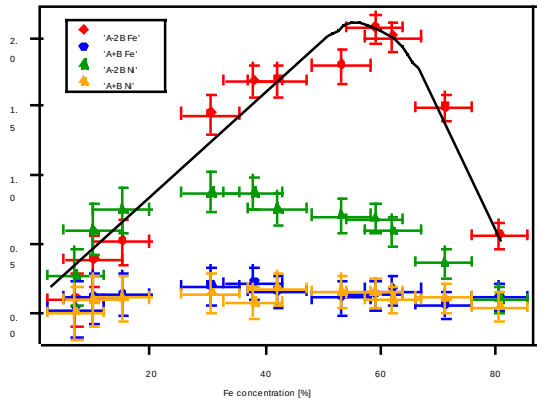


Figure 2. The variations of the spin, respectively orbital parts of the magnetic moments. [A-2B=-C/$\mu_B(\mu_s+\mu_D^{\alpha})$; A+B=-3C/2$\mu_B(\mu_O^{\alpha})$]. A, B are the areas underneath the difference peaks of the 2p spectra taken with magnetization up and down.

## REFERENCES


1. C.E. Guillaume, C.R. Acad. Sci. **125**, 235 (1897)
2. E.F. Wassermann in "Ferromagnetic Materials", Vol. 5, K.H. Buchow & E.P. Wohlfarth (eds.), Elsevier, Amsterdam (1990)
3. R.J. Weiss, Proc. R. Soc. London, Sect. A **82**, 281 (1963)
4. M. van Schilfgaarde, I.A. Abrikosov and B. Johansson, Nature 400, 46 (1999)
5. I.A. Abrikosov, O. Erikson, P. Sonderling, H.L, Skriver, & B. Johansson, Phys. Rev. B51,1058 (1995)
6. F.O. Schumann, R.F. Willis, K.G. Goodman, & J.G. Tobin, Phys. Rev. Lett. **79**, 5166 (1997)
7. J.W. Freeland, I.L. Grigorov, & J.C. Walker, Phys. Rev. **B57**, 80 (1998)
8. M. Hochstrasser, N. Gilman, R.F. Willis, F.O. Schumann, J.G. Tobin, & E. Rotenberg, Phys. Rev. **B60**, 17030 (1999)
9. D.Y. Petrovykh, K.N. Altmann, H. Höchst, M. Laubscher, S. Maat, G.J. Mankey, & F.J. Himpsel, Appl. Phys. Lett. **73**, 3459 (1998)
10. "Ferromagnetism" by R.M. Bozorth, Van Nostrand (1951)



This work was supported by the Director, Office of Energy Research, Office of Basic Energy Sciences, Materials Science Division, of the U.S. Department of Energy under Contract No. *# R5-32633.A02*. This work was performed under the auspices of the U.S Department of Energy by Lawrence Livermore National Laboratory under contract no. W-7405-Eng-48. Experiments were carried out at the Spectromicroscopy Facility (Beamline 7.0) and at Beamline 4 at the Advance Light Source, built and supported by the Office of Basic Energy Science, U.S. Department of Energy.



Principal investigator: J.G. Tobin, Chemistry & Material Science Division, Lawrence Livermore National Laboratory, Livermore, California 94550, USA, Email: tobin1@llnl.gov, Telephone: 925 422 7247